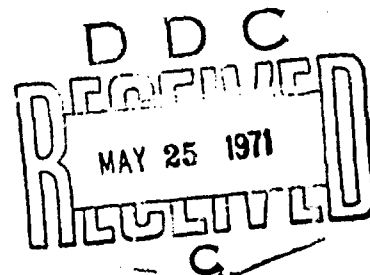# Magnetic structure of skew ionizing shock waves

By B. P. LEONARD

Plasma Laboratory, Columbia University, New York

1

DOCUMENT CONTROL DATA - R & D

(Security classification of title, body of abstract and indexing annotation must be entered when the overall report is classified)

1. ORIGINATING ACTIVITY *(Corporate author)*	2a. REPORT SECURITY CLASSIFICATION
COLUMBIA UNIVERSITY	UNCLASSIFIED
PLASMA LABORATORY - SCHOOL OF ENGR & APPLIED SCIENCE	2b. GROUP
NEW YORK, NEW YORK 10027	

3. REPORT TITLE

MAGNETIC STRUCTURE OF SKEW IONIZING SHOCK WAVES

4. DESCRIPTIVE NOTES *(Type of report and inclusive dates)*
Scientific   Interim

5. AUTHOR(S) *(First name, middle initial, last name)*

B P LEONARD

6. REPORT DATE	7a. TOTAL NO. OF PAGES	7b. NO. OF REFS
July 1970	51	10

8a. CONTRACT OR GRANT NO.	9a. ORIGINATOR'S REPORT NUMBER(S)
AF 49(638)-1634	
b. PROJECT NO.	REPORT NO. 49
9752-01	
c. 61102F	9b. OTHER REPORT NO(S) *(Any other numbers that may be assigned this report)*
681308	
d.	AFOSR-TR- 71-T 80 9

10. DISTRIBUTION STATEMENT

1. This document has been approved for public release and sale; its distribution is unlimited.

11. SUPPLEMENTARY NOTES	12. SPONSORING MILITARY ACTIVITY
	AF Office of Scientific Research (NAE)
TECH, OTHER	1400 Wilson Boulevard
	Arlington, Virginia 22209

13. ABSTRACT

Initially nonconducting gas is ionized by a thin viscous shock wave. Upstream there can be no magnetohydrodynamic interaction because of the zero conductivity, but the conducting downstream region may have a magnetic structure which interacts with the flow variables. A theoretical analysis is made in the zero-magnetic-Prandtl-number ("non-viscous") limit, i.e., Ohmic dissipation is the dominant diffusion mechanism. Unlike magnetohydrodynamic shocks in a pre-ionized gas, ionizing shock waves are not necessarily plane-polarized. Thus "skew" shock structures can exist, in which the upstream and downstream magnetic field vectors and the shock wave normal do not all lie in a single plane. The existence of the viscous subshock at the front of the magnetic layer requires the upstream Mach number to be greater than unity. Explicit solutions are given for typical values of the governing parameters, showing how the magnetic field vector rotates about the shock wave normal as its transverse component changes in magnitude through the shock layer. Skew shocks are necessarily sub-Alfvénic downstream. Unlike the pre-ionized case, the range of trans-Alfvénic shock waves is not excluded, since these shocks can absorb Alfvén waves within their structure. With strong magnetic fields it is possible to achieve very high downstream temperatures by Joule heating. Alternatively, in some cases, magnetic energy can be fed into directed kinetic energy, producing an overall expansion shock.

DD FORM 1473
, NOV 65

KEY WORDS	LINK A		LINK B		LINK C	
	ROLE	WT	ROLE	WT	ROLE	WT
SHOCK WAVE STRUCTURE						
MAGNETIC STRUCTURE						
IONIZING SHOCK WAVES						
OHMIC DISSIPATION						
SKEW SHOCK STRUCTURE						
TRANS-ALFVÉNIC SHOCK WAVES						
JOULE HEATING						

CONTENTS

ABSTRACT

Initially nonconducting gas is ionized by a thin viscous shock wave. Upstream there can be no magnetohydrodynamic interaction because of the zero conductivity, but the conducting downstream region may have a magnetic structure which interacts with the flow variables. A theoretical analysis is made in the zero-magnetic-Prandtl-number ("non-viscous") limit, i.e., Ohmic dissipation is the dominant diffusion mechanism. Unlike magnetohydrodynamic shocks in a pre-ionized gas, ionizing shock waves are not necessarily plane-polarized. Thus "skew" shock structures can exist, in which the upstream and downstream magnetic field vectors and the shock wave normal do not all lie in a single plane. The existence of the viscous subshock at the front of the magnetic layer requires the upstream Mach number to be greater than unity. Explicit solutions are given for typical values of the governing parameters, showing how the magnetic field vector rotates about the shock wave normal as its transverse component changes in magnitude through the shock layer. Skew shocks are necessarily sub-Alfvénic downstream. Unlike the pre-ionized case, the range of trans-Alfvénic shock waves is not excluded, since these shocks can absorb Alfvén waves within their structure. With strong magnetic fields it is possible to achieve very high downstream temperatures by Joule heating. Alternatively, in some cases, magnetic energy can be fed into directed kinetic energy, producing an overall expansion shock.

1. Introduction

This article concerns the magnetic structure of ionizing shock waves when Ohmic dissipation is the dominant diffusion mechanism. Viscous and heat conduction effects are neglected in the magnetic shock layer, and are important only in an infinitely thin subshock, which is assumed to exist at the front of the magnetic layer. This subshock is responsible for ionizing the previously non-ionized upstream gas so that it becomes an electrical conductor somewhere within the subshock, and remains conducting everywhere downstream. As will be shown in § 2.3, the detailed variation of the (scalar) electrical conductivity, although important in the full analysis of the problem, can be suppressed by a suitable nonuniform "stretching" of the normal space coordinate. The initial analysis is thus equivalent to that of a hypothetical gas which has zero conductivity upstream of the subshock, and __constant__ (finite) conductivity everywhere downstream. The neglect of subshock fine-structure means that the present analysis is the "outer expansion" in a matched asymptotic expansion procedure as described, for example, by Van Dyke (1964). The inner expansion and matched composite solution, together with the analysis of the stretching effects of variable conductivity (due to variations in the degree of ionization and in the electron temperature) will be presented at a later date.

Several parameters govern the behaviour of ionizing shock waves. Naturally it is not feasible to present details for a

full range of all the parameters. For this reason, only cases of infinite upstream Mach number M_1 will be considered, i.e., [flow kinetic energy] $\gg$ [thermal energy], upstream. For Mach numbers above $M_1 \sim 20$, this is certainly a good approximation, because the thermal terms which are neglected in the analysis are $\underline{0}(M_1^{-2})$.

The shock wave normal defines one direction (e.g., the x axis, say). Perpendicular to this, the constant transverse electric field defines another suitable reference direction (e.g., the z axis, say). The other mutually perpendicular transverse direction (y axis) completes a Cartesian coordinate system. The special cases of "normal" shock waves (no upstream transverse magnetic field components) and "oblique" shock waves (the upstream magnetic field has finite x and y components, but no z component) will be considered in a subsequent paper [Leonard, (1970b)]. "Skew" shock waves (in which the upstream magnetic field involves all three components) will be discussed here, but, primarily, for only one set of upstream angles (see § 3). The term "skew" seems to be appropriate for this latter type of shock: whereas, in normal and oblique shock waves, the upstream and downstream magnetic field vectors and the shock wave normal lie in a single plane, in skew shocks they do not. Hence skew shocks represent the most general type of geometrical configuration. The possibility of such shock waves was mentioned, in passing, by Cowley (1967), who, however, confined his attention to the more commonly studied cases involving only a single

transverse component. As will be shown in the companion paper, in oblique shocks, the magnetic field vector lies in a single plane throughout the entire shock structure, provided the conductivity is a scalar. Hence oblique shocks are always plane-polarized. This is also true of normal shocks. The structure of "transverse" ionizing shock waves (no normal magnetic field component) is discussed in Appendix 1 of that paper, where it is shown that such shocks must always be of the magnetically-trivial gas shock variety, when Ohmic dissipation is the only significant diffusion mechanism.

It will be shown in § 3.3 that skew shocks are necessarily sub-Alfvénic downstream. Skew shocks which are entirely sub-Alfvénic always have a range of structures, uniquely determined by the strength of the transverse electric field, which is taken to be a free parameter. Unique structures can also be found for a range of (trans-Alfvénic) shock waves in which the upstream region is super-Alfvénic, i.e., unity-local-Alfvén-number occurs within the shock structure. The fact that these trans-Alfvénic ionizing shock waves are stable to rotational Alfvén disturbances (in constrast to the anomalous trans-Alfvénic "solutions" in the pre-ionized case) has been discussed previously [Leonard, (1970a)]. In terms of typical ionizing shock structure behaviour, there is, in fact, no significant distinction between the trans-Alfvénic and completely sub-Alfvénic regimes.

In the next section, the governing equations will be developed. The behaviour is governed by two first-order differential

equations for the transverse magnetic field components, with auxiliary variables being defined algebraically. An integral coordinate transformation decouples the basic equations from variable-conductivity effects. In § 3, typical behaviour of the solutions is discussed with particular reference to the parametric variation of the electric field strength. Optimization of the electric field for the achievement of maximum downstream temperature is also discussed. It appears that the conversion of magnetic energy into thermal energy by Joule heating can be responsible for raising the downstream temperature by a factor of several times the downstream subshock temperature. Under certain circumstances, magnetic energy can be converted into directed kinetic energy in the magnetic layer, so that after an initial (viscous) compression, a re-expansion takes place downstream, giving the possibility (for relatively large upstream magnetic pressure ratios) of overall expansion shocks.

In the examples of § 3 and the Appendix, all results are obtained by exact numerical evaluation of algebraic expressions or by numerical integration of the governing differential equations.

2. Governing equations

2.1 Physical laws

It is assumed that a shock-fixed coordinate system can be chosen such that the shock structure becomes steady and one-dimensional. Dimensional variables carry a bar. The $\bar{x}$ coordinate is taken as the single independent variable, which is positive downstream, with its origin at the subshock. Uniform conditions $(d/d\bar{x} \rightarrow 0)$ are assumed far upstream $(\bar{x} = -\infty)$ where, for the moment, completely general conditions are assumed for the velocity $\underline{\bar{v}}_1 = [\bar{v}_{x1}, \bar{v}_{y1}, \bar{v}_{z1}]$, magnetic field $\underline{\bar{B}}_1 = [\bar{B}_{x1}, \bar{B}_{y1}, \bar{B}_{z1}]$, and electric field $\underline{\bar{E}}_1 = [\bar{E}_{x1}, \bar{E}_{y1}, \bar{E}_{z1}]$. A transition to uniform downstream conditions (as $\bar{x} \rightarrow +\infty$) given by $\underline{\bar{v}}_2$, $\underline{\bar{B}}_2$, and $\underline{\bar{E}}_2$, is sought. The most symmetrical form of the governing equations seems to arise if the coordinate system is chosen such that the downstream $\underline{\bar{B}}$ field and velocity are in the same plane [the $(\bar{x}, \bar{y})$ plane, say]. This can always be done as follows:

(i) Rotation about the $\bar{x}$ axis $\rightarrow \underline{\bar{B}}_2 = [\bar{B}_{x2}, \bar{B}_{y2}, 0]$;

(ii) Translation parallel to the $\bar{z}$ axis $\rightarrow \underline{\bar{v}}_2 = [\bar{v}_{x2}, \bar{v}_{y2}, 0]$, since a Galilean transformation does not change the magnetic field in a nonrelativistic theory.

A translation parallel to the $\bar{y}$ axis is still available. This is chosen so that the upstream velocity can be taken as $\underline{\bar{v}}_1 = [\bar{v}_{x1}, 0, \bar{v}_{z1}]$ for convenience. In general the upstream magnetic field may have three nonzero components. The form of

the electric field can be determined from Ohm's law for the conduction current density $\underset{\sim}{J}$,

$$\underset{\sim}{J} = \overline{\sigma}[\underset{\sim}{E} + \underset{\sim}{\overline{v}} \times \underset{\sim}{\overline{B}}], \qquad (1)$$

where $\overline{\sigma}$ is the scalar electrical conductivity. Ampere's equation in the steady state gives

$$\underset{\sim}{\overline{\nabla}} \times (\underset{\sim}{\overline{B}}/\mu) = \underset{\sim}{J} + \overline{\rho}_c \underset{\sim}{\overline{v}} \approx \underset{\sim}{J}, \qquad (2)$$

where μ is the magnetic permeability, and ρ_c is the negligibly small charge density. Applied in the downstream uniform region, where it is assumed that $\overline{\sigma}_2 \neq 0$, equations (1) and (2) require

$$\underset{\sim}{E}_2 = - \underset{\sim}{\overline{v}}_2 \times \underset{\sim}{\overline{B}}_2, \qquad (3)$$

so, in the chosen coordinate system, $\underset{\sim}{E}_2 = [0,0,\overline{E}_{z2}]$. Faraday's law in the steady case requires $\overline{\nabla} \times \underset{\sim}{\overline{E}} = \underset{\sim}{0}$; thus the transverse components of $\underset{\sim}{E}$ are constant throughout the shock layer: $\overline{E}_y(\overline{x}) \equiv 0$, and $\overline{E}_z(\overline{x}) = \overline{E}_{z2} = \overline{E}_z$, say. At this stage, no preliminary information is available on $\overline{E}_x$ (Poisson's equation merely implies that the charge density will be extremely small), hence the electric field can be written as

$$\underset{\sim}{E}(\overline{x}) = [\overline{E}_x(\overline{x}), 0, \overline{E}_z]. \qquad (4)$$

The solenoidal condition, $\underline{\bar{\nabla}} \cdot \underline{\bar{B}} = 0$, requires the constancy of the normal magnetic field component, $\bar{B}_x(\vec{x}) \equiv \bar{B}_x = \text{const.}$ The transverse components are variable, hence

$$\underline{\bar{B}}(\vec{x}) = [\bar{B}_x, \bar{B}_y(\vec{x}), \bar{B}_z(\vec{x})]. \tag{5}$$

Viscous and heat conduction terms will be neglected unless the gradients of velocity and temperature become "infinite" (i.e., when these variables change by order unity in a length which is very small compared with the "magnetic" length scale). This is the zero-magnetic-Prandtl-number approximation:

$$Pm = \mu \bar{\sigma} \bar{\nu} \to 0, \tag{6}$$

where $\bar{\nu}$ is the kinematic viscosity. In this limit, the Ohmic diffusion length resulting from the nonzero electrical resistivity $(= \bar{\sigma}^{-1})$, is larger than diffusion lengths of the relatively small viscosity or heat conductivity. Mathematically this leads to the previously mentioned outer expansion in a matched asymptotic expansion procedure in terms of a small[†] parameter Pm. It must be stressed that the discontinuities appearing in the

---

[†] In the author's experience in other analyses (Leonard, 1969), matched first-order composite solutions give very "reasonable" results even when the perturbation parameter is as large as one-third.

present solutions can (in principle) be resolved by using suitable inner expansions and matching to form uniformly valid composite solutions; but this will not be attempted here.

For steady flow, the mass, momentum, and energy conservation equations can be written, respectively

$$\underline{\nabla} \cdot (\overline{\rho} \underline{v}) = 0, \tag{7}$$

$$\underline{\nabla} \cdot \{\overline{\rho v v} - \underline{\overline{BB}}/\mu + [\overline{p} + \overline{B}^2/(2\mu)]\underline{\mathcal{I}}\} = \underline{0}, \tag{8}$$

$$\underline{\nabla} \cdot [(\overline{\rho u} + \tfrac{1}{2}\overline{\rho v}^2)\underline{v} + \overline{p}\underline{v} + (\underline{E} \times \underline{B})/\mu] = 0, \tag{9}$$

where $\overline{\rho}$ is the density, $\overline{p}$ the pressure, and $\overline{u}$ the specific internal energy. Electrostatic terms have been ignored for reasons explained by Shercliff (1965). For convenience, ideal gas state and internal energy relations are assumed, introducing the effective[†] gas temperature $\overline{T}$:

$$\overline{p} = \overline{\rho}R\overline{T}, \tag{10}$$

and

$$\overline{u} = R\overline{T}/(\gamma-1), \tag{11}$$

where R is the gas constant and γ the specific heat ratio.

[†]As used here, $\overline{T} = \overline{T}_h + \alpha\overline{T}_e$, where "h" refers to heavy particles, "e" to electrons, and α is the degree of ionization. Note that this is not the overall temperature, $\overline{T}_{oa} = \overline{T}/(1+\alpha)$.

Ionization energy[†] has been neglected because only large-Mach-number cases will be studied.

2.2 Nondimensional equations

Appendix 1 of a subsequent paper [Leonard, (1970b)] considers the case of purely transverse ionizing shock waves $(\overline{B}_x = 0)$. Thus it is necessary here to consider only those shocks for which $\overline{B}_x \neq 0$. This component is therefore used in the nondimensionalization of the following: $\underset{\sim}{B} = \overline{\underset{\sim}{B}}/\overline{B}_x$, $\underset{\sim}{v} = \overline{\underset{\sim}{v}}/\overline{v}_{x1}$, $\underset{\sim}{E} = \overline{\underset{\sim}{E}}/(\overline{v}_{x1}\overline{B}_x)$ $\rho = \overline{\rho}/\rho_1$, and $T = \overline{T}/\overline{T}_1$. Equations (7), (8), and (9) take the integrated one-dimensional forms [using equations (10) and (11)].

$$\rho v_x = \text{const.}[1] = 1, \tag{12}$$

(this has been used in the following)

$$v_x + \frac{T}{v_x \gamma M_1^2} + \tfrac{1}{2}\alpha_{x1}^2 (B_y^2 + B_z^2) = \text{const.}[1]$$

$$= 1 + \frac{1}{\gamma M_1^2} + \tfrac{1}{2}\alpha_{x1}^2 (B_{y1}^2 + B_{z1}^2), \tag{13}$$

$$v_y - \alpha_{x1}^2 B_y = \text{const.}[1] \tag{14}$$

$$v_z - \alpha_{x1}^2 B_z = \text{const.}[2] = 0, \tag{15}$$

[†]This term, $\sim\alpha/M_1^2$, could be formally kept, but the (weak) coupling with α introduces mathematical complications which disappear when $M_1^2 \to \infty$.

and

$$\frac{T}{M_1^2(\gamma-1)} + \tfrac{1}{2}(v_x^2 + v_y^2 + v_z^2) - \alpha_{x1}^2 E_z B_y = \text{const.}[1]$$

$$= \frac{1}{M_1^2(\gamma-1)} + \tfrac{1}{2}(1 + \alpha_{x1}^4 B_{z1}^2) - \alpha_{x1}^2 E_z B_{y1}, \qquad (16)$$

where the x component magnetic pressure ratio is

$$\alpha_{x1}^2 = (\overline{B}_x^2/\mu)/(\overline{\rho}_1 \overline{v}_{x1}^2) = 1/A_1^2, \qquad (17)$$

(A_1 being the shock Alfvén number), and the shock Mach number M_1 is given by

$$\gamma M_1^2 = \overline{v}_{x1}^2/(R\overline{T}_1). \qquad (18)$$

Note that equation (15) requires the z components of the velocity and magnetic field to be proportional throughout the shock layer. In particular this must be true upstream; this fact has been used in replacing v_{z1}^2 by $\alpha_{x1}^4 B_{z1}^2$ on the right hand side of equation (16). The constants appearing in these fluid equations have been evaluated in the regions shown in square brackets; they are seen to depend on the parameters: γ, M_1^2, α_{x1}^2, B_{y1}, B_{z1}, and E_z. Equations (13) — (16) are invalidated if gradients of velocity and temperature become very large as in the viscous subshock, however these equations must be satisfied immediately in front of and behind the subshock.

If $\underline{J}$ is eliminated between equations (1) and (2) the nondimensional component equations become

$$J_x = Rm(E_x + v_y B_z - v_z B_y) = -\rho_c v_x \approx 0, \qquad (19)$$

$$J_y = -dB_z/d\tilde{x} = Rm(v_z - v_x B_z), \qquad (20)$$

and

$$J_z = dB_y/d\tilde{x} = Rm(E_z + v_x B_y - v_y), \qquad (21)$$

where $\underline{J} = \overline{J}/[\overline{B}_x/(\mu \mathcal{l}_R)]$, $\tilde{x} = \overline{x}/\mathcal{l}_R$, and a quasi-local magnetic magnetic Reynolds number $Rm(\tilde{x}) = [\mu \overline{v}_{x1} \mathcal{l}_R] \overline{\sigma}(\tilde{x})$ has been introduced using a reference length $\mathcal{l}_R$ which is as yet unspecified. [$Rm(\tilde{x})$ can be regarded as a nondimensionalized conductivity.] In equation (19) the extremely small charge density $\rho_c = \overline{\rho}_c/[\overline{B}_x/(\mu \mathcal{l}_R \overline{v}_{x1})]$ has been included for later reference, but has been completely neglected in equations (20) and (21).

Recall that $\overline{\sigma}$ (and hence Rm) is proportional to the degree of ionization and inversely proportional to the electron-heavy particle collision frequency, which depends on the local (non-equilibrium) electron temperature. This coupling with ionization and electron temperature effects (which may occur over a length scale comparable to the magnetic length because of ionization lags and non-equilibrium Joule heating of the electrons) can be suppressed by the coordinate transformation

of § 2.3. Hence it is not necessary at this stage to give
explicit equations describing the electron temperature behaviour
and the ionization dynamics. Note however that it will be as-
sumed that $\bar{\sigma}$, which is zero upstream, does have some finite
value everywhere on the downstream side $(\tilde{x} > 0_+)$ of the vis-
cous subshock. In addition, precursor ionization, if it exists,
will be assumed to be confined to a length scale comparable
to the viscous length, or else to be of such small magnitude
that significant magnetic effects do not occur upstream of the
subshock. (The upstream change in magnetic field is proportion-
al to the precursor ionization length scale times some average
degree of ionization; thus the solutions of the present analysis
are applicable only to those cases for which this product is
small.)

Substituting equations (14) and (15) into equation (19)
gives

$$Rm[E_x + \alpha_{x1}^2 (B_y - B_{y1})B_z - \alpha_{x1}^2 B_z B_y] \approx C, \qquad (22)$$

i.e.,

$$Rm[E_x - (\alpha_{x1}^2 B_{y1})B_z] \approx 0. \qquad (23)$$

Upstream (where Rm = 0) this is automatically satisfied.
Note that equation (20) requires B_z= const.= B_{z1} everywhere
upstream, but equation (23) still allows $E_x(\tilde{x}<0)$ to be

arbitrary. Downstream, Rm is nonzero, so equation (23) requires

$$E_x \approx (\alpha_{x1}^2 B_{y1}) B_z, \quad \tilde{x} > 0, \tag{24}$$

and from Poisson's equation the charge density ρ_c is proportional to the derivative of this, which in turn is proportional to J_y [from equation (20)]. To an excellent approximation the nondimensional relationship is

$$\rho_c = (\overline{v}_{x1}/\overline{c})^2 dE_x/d\tilde{x} = (\overline{v}_{x1}/\overline{c})^2 \alpha_{x1}^2 B_{y1} J_y, \tag{25}$$

where $\overline{c}$ is the electromagnetic propagation speed. This extremely small charge density is caused by insignificant deviation of E_x from the value given by equation (24) [solve for ρ_c in equation (19)].

In the general case, $\underline{B}_1 = [1, B_{y1}, B_{z1}]$, $\underline{v}_1 = [1, 0, \alpha_{x1}^2 B_{z1}]$, equations (20) and (21) require that upstream (where $Rm = 0$) and across the subshock: $\underline{B}(\tilde{x} \leq 0_+) \equiv \underline{B}_1$. Since $\underline{B}$ does not vary upstream, there can be no magnetohydrodynamic interaction on the fluid variables, so $\underline{v}(\tilde{x} < 0_-) \equiv \underline{v}_1$; but note that across the subshock, $\tilde{x} = 0_- \rightarrow 0_+$, $\underline{v}$ changes discontinuously. In the downstream magnetic layer $\underline{B}$ and $\underline{v}$ may change continuously in magnitude and in both direction angles, finally approaching the uniform downstream state in which $\underline{B}_{z2} = \underline{v}_{z2} = 0$. Clearly neither the magnetic field vector nor the velocity vector lies in a single plane in the general case of skew shocks.

The above discussion assumes that the electrical conducti-vity is a <u>scalar</u>. When Hall currents are present in <u>conducting-upstream</u> shock waves, as described by Leonard (1966), $\underline{B}$ and $\underline{v}$ contain spiralling components in the (y,z) plane, although their upstream and downstream limits must lie in a single plane with the shock wave normal. This spiralling behaviour is also expected to occur in <u>ionizing</u> shocks (whether skew, oblique or normal), when Hall currents are important, but will not be considered here, i.e., it will be assumed that $\bar{\sigma}$ is a scalar.

Equations (20) and (21) are the fundamental "magnetic" equations for the structure of the transverse magnetic field components in the downstream shock layer. The coupling with the <u>transverse</u> velocity components can be eliminated explicitly by using equations (14) and (15), giving

$$\frac{dB_y}{d\tilde{x}} = Rm[E^* - (\alpha_{x1}^2 - v_x)B_y], \tag{26}$$

and

$$\frac{dB_z}{d\tilde{x}} = - Rm(\alpha_{x1}^2 - v_x)B_z, \tag{27}$$

where

$$E^* = E_z + \alpha_{x1}^2 B_{y1} = const. \tag{28}$$

It is notationally convenient to leave the coupling with v_x in these equations although, in fact, $v_x = v_x\{B_y, B_z\}$ in the magnetic layer, which means that equations (26) and (27) are implicitly coupled.

If v_y, v_z, and T are eliminated from equations (13) — (16), the relationship between v_x, B_y, and B_z can be found; in an implicit form it is

$$f(v_x, B_y, B_z)$$

$$= \alpha_{x1}^2 \left[\frac{\gamma v_x}{\gamma-1} - \alpha_{x1}^2 \right] \left[(B_y - B_{y1})(B_y + B_{y1} - 2B_{y\mathcal{L}}) + B_z^2 - B_{z1}^2 \right]$$

$$+ \frac{(\gamma+1)}{(\gamma-1)} (v_x - 1)(v_x - v_x^*) = 0, \tag{29}$$

where

$$B_{y\mathcal{L}} = B_{y\mathcal{L}}(v_x) = \frac{E^*}{[\alpha_{x1}^2 - \gamma v_x / (\gamma-1)]}, \tag{30}$$

and where the downstream subshock velocity v_x^* is

$$v_x^* = v_x(\tilde{x} = 0_+) = (\gamma - 1 + 2/M_1^2)/(\gamma+1). \tag{31}$$

Note that, everywhere upstream and across the subshock, $B_y = B_{y1}$, and $B_z = B_{z1}$, hence equation (29) requires $v_x = 1$ (for $\tilde{x} \le 0_-$), or $v_x = v_x^*$ (for $\tilde{x} = 0_+$).

Equation (29) represents a surface $f = 0$ in (v_x, B_y, B_z) space, It can be rearranged as

$$(B_y - B_{y\rlap{/}\ell})^2 + B_z^2$$

$$= (B_{y1} - B_{y\rlap{/}\ell})^2 + B_{z1}^2 + \frac{(\gamma+1)(v_x-1)(v_x-v_x^{\star})}{\alpha_{x1}^2[\alpha_{x1}^2(\gamma-1)-\gamma v_x]} . \qquad (32)$$

In this form, it can be seen that planes $v_x = \text{const.}$ intersect the surface in circles with centres at $B_y = B_{y\rlap{/}\ell}(v_x)$, $B_z = 0$, and of radius equal to the square root of the right hand side of the equation (32). From equation (30) the "centreline" curve is seen to be a hyperbola in the (v_x, B_y) plane with an asymptote at $v_x^A = \alpha_{x1}^2(\gamma-1)/\gamma$. The radius also has a singularity at this value. Note that $f = 0$ contains the upstream point $[v_x=1, B_y=B_{y1}, B_z=B_{z1}]$, and the subshock downstream point $[v_x=v_x^{\star}, B_y=B_{y1}, B_z=B_{z1}]$.

In § 2.3 a new space coordinate x is introduced which eliminates the variable-Rm factors in equations (26) and (27); thus $B_y(x)$ and $B_z(x)$ can be found by direct simultaneous (numerical) integration, the normal velocity $v_x(x)$ being computed from equation (29) as the integration proceeds. The density is $\rho(x) = 1/v_x$, from equation (12). Equations (14) and (15) give the transverse velocity components $v_y(x) = \alpha_{x1}^2(B_y - B_{y1})$, and $v_z = \alpha_{x1}^2 B_z$. Equation (13) can be rearranged to give the temperature

$$T = v_x\{1 + \gamma M_1^2[1 - v_x - \tfrac{1}{2}\alpha_{x1}^2(B_r^2 - B_{r1}^2)]\}, \tag{33}$$

where $B_r^2 = B_y^2 + B_z^2$. A decrease in the transverse magnitude B_r corresponds to a conversion of magnetic energy into thermal energy. The nondimensional pressure and internal energy are given, respectively, by

$$p \equiv \overline{p}/(\overline{\rho}_1\overline{v}_{x1}^2) = T/(v_x\gamma M_1^2), \tag{34}$$

and

$$u \equiv \overline{u}/\overline{v}_{x1}^2 = T/[\gamma M_1^2(\gamma-1)]. \tag{35}$$

For steady flow, and in the absence of viscous dissipation and thermal conduction (i.e., in the magnetic layer, but not in the subshock), the dimensional entropy equation given by Shercliff (1965) becomes

$$\overline{\rho}_1\overline{v}_{x1}\frac{d\overline{s}}{d\overline{x}} = \frac{\overline{J}^2/\overline{\sigma}}{\overline{T}}$$

$$= \frac{1}{\overline{T}}\left[\left(\frac{1}{\mu}\frac{d\overline{B}_y}{d\overline{x}}\right)(\underline{E}+\underline{v}\times\underline{B})_z - \left(\frac{1}{\mu}\frac{d\overline{B}_z}{d\overline{x}}\right)(\underline{E}+\underline{v}\times\underline{B})_y\right], \tag{36}$$

where all the entropy production is due to Ohmic dissipation. The nondimensional form of this equation is discussed in the next section where the entropy s is given as an explicit

integral involving B_y, B_z, v_x, and T.

Finally, it is sometimes convenient to rescale the temperature in terms of the viscous temperature $T^* = T(\tilde{x}=0_+)$, which, from equation (33), with $B_r = B_{r1}$, and $v_x = v_x^*$, is

$$T^* = v_x^*[1 + \gamma M_1^2(1-v_x^*)]$$

$$= \frac{2\gamma(\gamma-1)}{(\gamma+1)^2} M_1^2\left[1 - \frac{(\gamma-1)}{2\gamma M_1^2}\right]\left[1 + \frac{2}{(\gamma-1)M_1^2}\right] . \tag{37}$$

Then the rescaled temperature is

$$\hat{T} \equiv T/T^*$$

$$= \frac{(\gamma+1)^2 v_x[1 - v_x + 1/(\gamma M_1^2) - \frac{1}{2}\alpha_{x1}^2(B_r^2-B_{r1}^2)]}{2(\gamma-1)[1 - (\gamma-1)/(2\gamma M_1^2)]\{1 + 2/[(\gamma-1)M_1^2]\}} . \tag{38}$$

In this form, the Mach number dependence of $\hat{T}$ is $\underline{O}(1)$.

2.3 Integral coordinate transformation

This analysis assumes that the electrical conductivity $\bar{\sigma}$ is identically zero from $\bar{x} = -\infty$ to $\bar{x} = 0_-$ (just upstream of the viscous subshock) and that, from $\bar{x} = 0_+$ (just downstream) to $\bar{x} = +\infty$, $\bar{\sigma}$ is finite and will, in general, vary with $\bar{x}$ (depending on the local values of the degree of ionization α and the electron temperature $\bar{T}_e$). Nondimensionally:

$Rm = Rm(\alpha, T_e)$, where α and T_e are functions of the space coordinate. Formally, equations (26) and (27) can be rewritten as

$$\frac{dB_y}{dx} = E^* - (\alpha_{x1}^2 - v_x)B_y,$$

$$= g_y(v_x, B_y), \quad \text{say}, \tag{39}$$

and

$$\frac{dB_z}{dx} = - (\alpha_{x1}^2 - v_x)B_z$$

$$= g_z(v_x, B_z), \quad \text{say}, \tag{40}$$

where a new space coordinate x has been introduced satisfying the differential relation

$$dx = Rm\, d\widetilde{x}, \quad \text{for } x, \widetilde{x} \geq 0_+, \tag{41}$$

locally. Equations (39) and (40) can be integrated [using the auxiliary equation (29)] to give $B_y = B_y(x)$ and $B_z = B_z(x)$, independently of the variation in α and T_e. The analysis is completed by finding α and T_e as functions of the _new coordinate_ x (using appropriate equations, not discussed here); then equation (41) is integrated (numerically) to give

$$\widetilde{x} = x(\widetilde{x}) = \int_o^x \frac{dx}{Rm[\alpha(x), T_e(x)]} \, , \qquad (42)$$

which can then be inverted to give $x = x(\widetilde{x})$. When this function is used in the arguments of the dependent variables, the latter are thus given as functions of the original nondimensional space coordinate $\widetilde{x}$; e.g., $B_y = B_y[x(\widetilde{x})]$, etc.

The only other equation to be affected by the coordinate transformation in the present case is that for the entropy, equation (36). This equation can be nondimensionalized to give

$$\frac{ds}{d\widetilde{x}} = \frac{\gamma M_1^2 \alpha_{x1}^2}{T} \left[\left(\frac{dB_y}{d\widetilde{x}}\right) g_y + \left(\frac{dB_z}{d\widetilde{x}}\right) g_z \right]$$

$$= \gamma M_1^2 \alpha_{x1}^2 \frac{Rm(g_y^2 + g_z^2)}{T} \, , \qquad (43)$$

where $s = \overline{s}/R$, and g_y and g_z are given by equations (39) and (40). The coordinate transformation $d\widetilde{x} = Rm^{-1} dx$ may now be applied and the Rm - factors cancelled, giving, on integration,

$$s = s(x) = \gamma M_1^2 \alpha_{x1}^2 \int_{o_+}^x \frac{(g_y^2 + g_z^2)}{T} dx + s(0_+). \qquad (44)^\dagger$$

Note that the factor, $\gamma M_1^2 \alpha_{x1}^2 = (\overline{B}_x^2/\mu)/(\overline{\rho}_1 R \overline{T}_1) = \beta_1^{-1}$, gives a measure of the ratio of the upstream magnetic pressure to the

---

†The gas subshock entropy jump gives $s(0_+) = \underline{0}(\log M_1^2)$.

gas pressure. However, for large Mach numbers, the downstream temperature, being the same order of magnitude as the viscous temperature $\bar{T}^*$, is $\underline{0}(M_1^2)$, so that $s \sim \alpha_{x1}^2$ rather than β_1^{-1}. In this case it is convenient to use the rescaled temperature $\hat{T}$, giving [from equations (37) and (38)], for $\Delta s_{MAG} \equiv s - s(0_+)$,

$$\Delta s_{MAG} = \frac{(\gamma+1)^2 \alpha_{x1}^2 \int_0^x [(g_y^2 + g_z^2)/\hat{T}]dx}{2(\gamma-1)[1 - (\gamma-1)/(2\gamma M_1^2)]\{1 + 2/[(\gamma-1)M_1^2]\}} . \qquad (45)$$

For small values of $\alpha_{x1}^2, \Delta s_{MAG} = \underline{0}(\alpha_{x1}^2)$, but for large values of α_{x1}^2, $\hat{T} \sim \alpha_{x1}^2$ [from equation (38)], so that $\Delta s_{MAG} = \underline{0}(1)$ in this case.

2.4 Mathematical formulation

The problem to be studied in this paper is summarized here, for reference. Shock structure profiles of $\underline{v}$, $\underline{B}$, $\hat{T}$, and Δs_{MAG} are required as functions of the __transformed__ space coordinate x. No attempt will be made to find $x(\tilde{x})$ in this report.

Given explicit values of the governing upstream parameters $[\gamma, M_1^2, \alpha_{x1}^2, B_{y1}, B_{z1}, E_z]$, the values of v^* and E^* can be computed using equations (28) and (31). The basic problem is to compute the downstream $(x \geq 0_+)$ magnetic structure $\underline{B}(x)$, using equations (39) and (40) [and the fact that $B_x = 1$] with equations (29) and (30) as auxiliary equations for $v_x(B_y, B_z)$. The initial conditions are those __just downstream of the subshock__

$(x = 0_+)$: $v_x = v_x^*$, $B_y = B_{y1}$, $B_z = B_{z1}$.   Except in isolated special cases, (numerical) integration of the two coupled first-order nonlinear differential equations for B_y and B_z can proceed from the subshock towards downstream infinity, at which point the system (usually) has a __nodal__ singularity. The other dependent variables, $v(x)$, $T(x)$, $\rho(x)$, $p(x)$, $u(x)$, and $s(x)$, can be computed from the respective algebraic or integral relations given by equations (29), (33), (12), (34), (35), and (44), or the equivalent relations for the thermodynamic variables involving the rescaled temperature $\hat{T}$.

Note that the downstream singular point $[(d/dx)_{+\infty} \to 0]$, which must lie on $f = 0$, is found from equations (39) and (40) to be given by the intersection of this surface with the hyperbola $g_z = g_y = 0$ [i.e., with $B_{z2} = 0$, $B_{y2} = E^*/(\alpha_{x1}^2 - v_{x2})$]. Since this point is in the (v_x, B_y) plane, it is found by the intersection of the hyperbola

$$B_y = \frac{E^*}{(\alpha_{x1}^2 - v_x)} \tag{46}$$

with the __plane__ __curve__ $f_0 = 0$ given by

$$
\begin{aligned}
f_c(v_x, B_y) &= f(v_x, B_y, 0) \\
&= \alpha_{x1}^2 \left[\frac{\gamma v_x}{\gamma-1} - \alpha_{x1}^2 \right] [\, (B_y - B_{y1})(B_y + B_{y1} - 2B_{y\xi}) - B_{z1}^2 \,] \\
&\quad + \frac{(\gamma+1)}{(\gamma-1)} (v_x - 1)(v_x - v_x^*) = 0,
\end{aligned}
\tag{47}
$$

from equation (29).

3. Skew shock structure

3.1 Typical behaviour

In (v_x, B_y, B_z) space, the structure trajectories of skew shocks start at $(1, B_{y1}, B_{z1})$, which is the upstream singular point corresponding to $x = -\infty$. This point is on the surface $f = 0$. Note that $dB_y/dx = dB_z/dx = 0$ at this point (and, in fact, everywhere upstream, $x \leq 0$) because $Rm(x \leq 0) = 0$ in equations (26) and (27), even though, in general, g_y and g_z [equations (39) and (40)] will be nonzero upstream. As x is increased from $-\infty$, everything remains constant at its upstream value until $x = 0_-$. From $x = 0_-$ to $x = 0_+$, the viscous subshock occurs. In (v_x, B_y, B_z) space, this is a straight line parallel to the v_x axis, starting at the upstream point and terminating at another point on $f = 0$ given by (v_x^*, B_{y1}, B_{z1}), where $v_x^* < 1$. At this point, Rm is no longer zero (by assumption), and as x is further increased, the trajectory moves away from the subshock point along an integral curve which lies entirely in the surface $f = 0$. As explained in the Appendix, this "magnetic" part of the trajectory must be on the <u>subsonic</u> sheet of $f = 0$ (whereas the upstream point is necessarily on the <u>supersonic</u> sheet); the <u>sonic</u> curve on $f = 0$ is the locus of points of tangency of lines parallel to the v_x axis. As $x \to +\infty$, the trajectory approaches the downstream (nodal[†]) singularity, given by the

---

[†]Except in isolated special cases, as explained in § 3.3, when the downstream subshock point lies exactly on the <u>saddle-point separatrix</u> [corresponding to a particular value of E^* $(=E_{MAX}^*)$].

intersection of the hyperbola $g_y = 0$ and the (v_x, B_y) plane
curve $f_o = 0$. The part of the solution trajectory on $f = 0$
is only one of a family of integral curves which densely cover
this surface. The Appendix discusses the topology of these
integral curves and some typical shapes of the surface $f = 0$
on which they lie.

Figure 1 shows two projections of the complete (v_x, B_y, B_z)
structure trajectory for a given set of parameters: $\gamma = 5/3$,
$M_1 = \infty$, $B_{y1} = 1$, $B_{z1} = 1$, $\alpha_{x1}^2 = 1.5$, and $E^* = -0.30$. The
corresponding structure profiles are shown in figure 2.
Figure 3 is a three-dimensional sketch of the behaviour of the
magnetic field vector throughout the shock layer, for this
typical skew shock. In this case, the value of E^* has been
chosen so that B_y changes sign. For other (positive) values
of E^*, this component may increase or decrease (but remain
positive). [The case $E^* = 0$ corresponds to a switch-off shock,
and, as explained in the Appendix, this type of shock is plane-
polarized, and should therefore properly be considered as belong-
ing to the family of oblique shocks rather than to that of skew
shocks[+].]

Another case, corresponding to the upstream and downstream
magnetic field vectors being at right angles $(B_{y1}=0, B_{z1}=1)$, is
portrayed by its trajectory projections in figure 4, for
$E^* = E_z > 0$. It is clear from symmetry considerations that,
for each solution for a given positive value of E_z, there is a

---

[+]For switch-off shocks there is no downstream datum for (y,z)-
orientation of the coordinate system, which may thus be chosen
so that $B_{z1} = 0$.
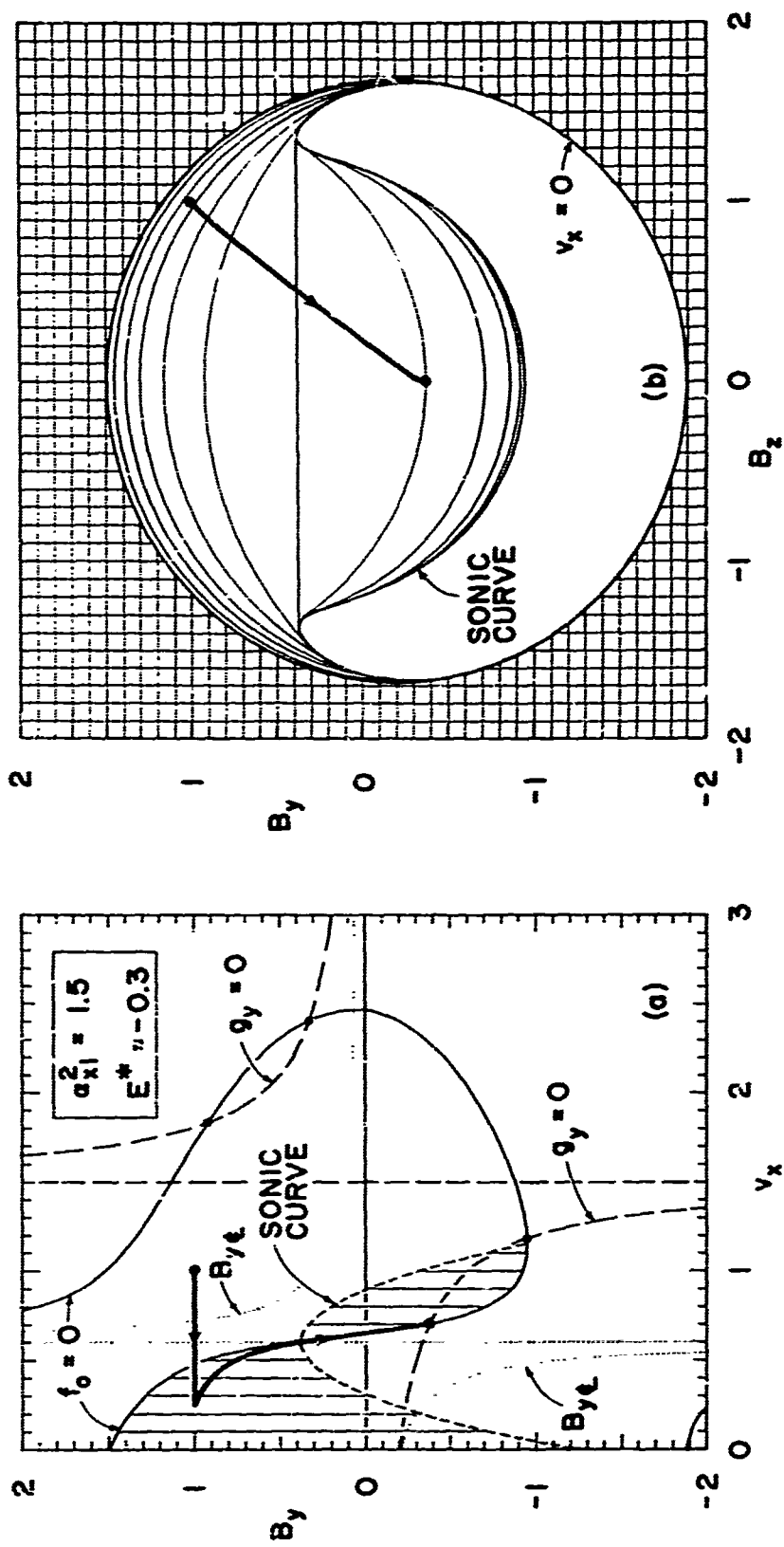
FIGURE 1. Two projections of a structure traject-
ory in (v_x, B_y, B_z) space shown in relation to
the surface $f = 0$, for the case $B_{y1} = 1$, $B_{z1} = 1$.
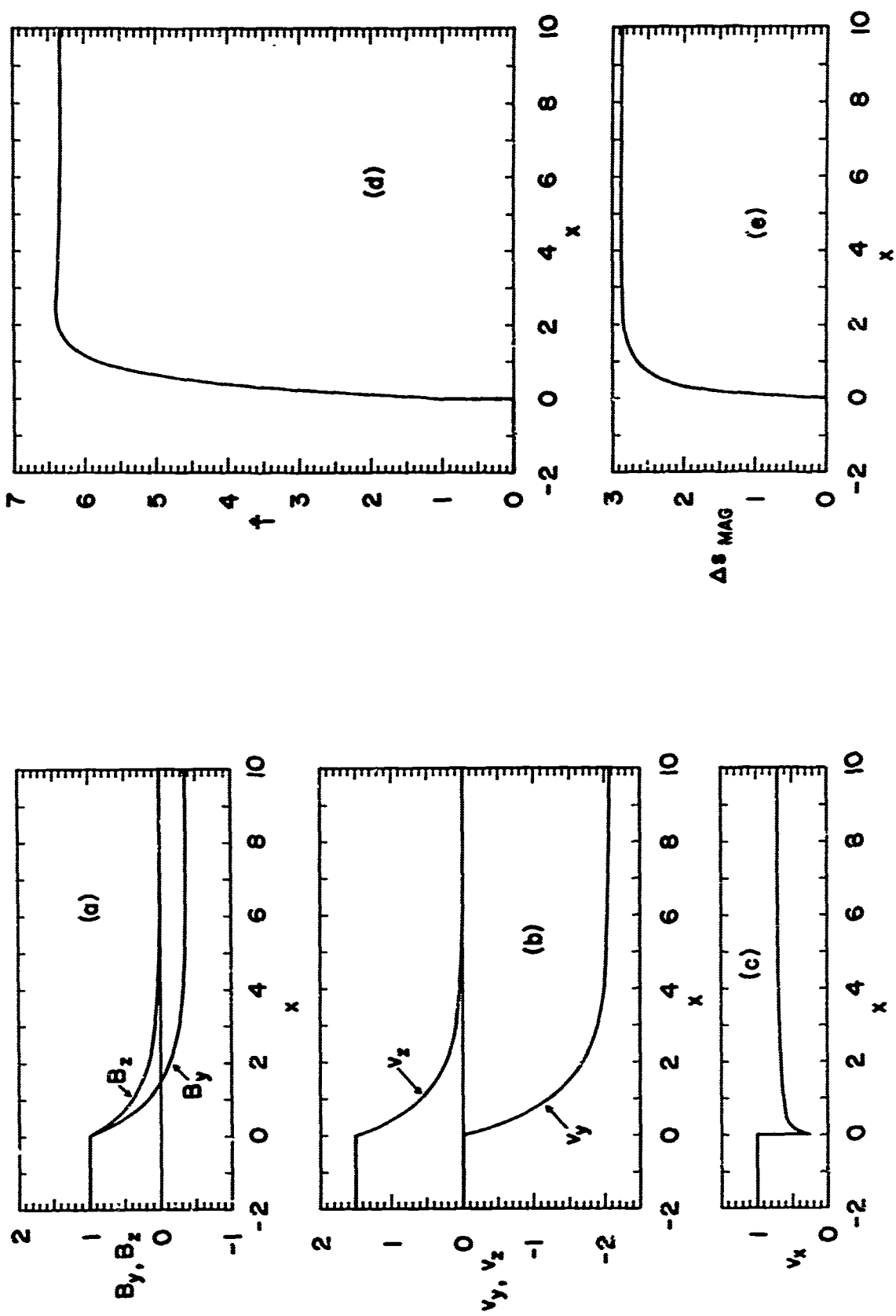
FIGURE 2. Shock structure profiles for the same parameters as in figure 1.
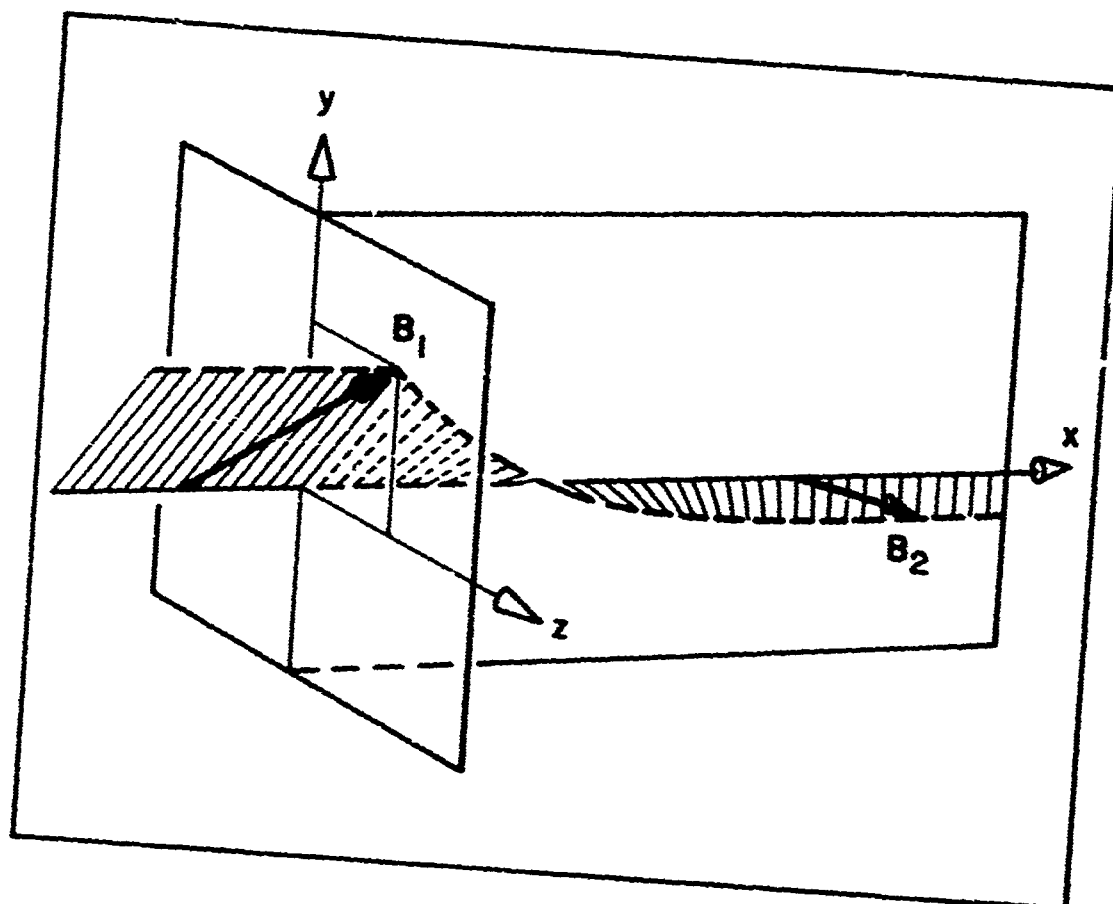
FIGURE 3. Three-dimensional representation of the
magnetic field vector variation through the shock
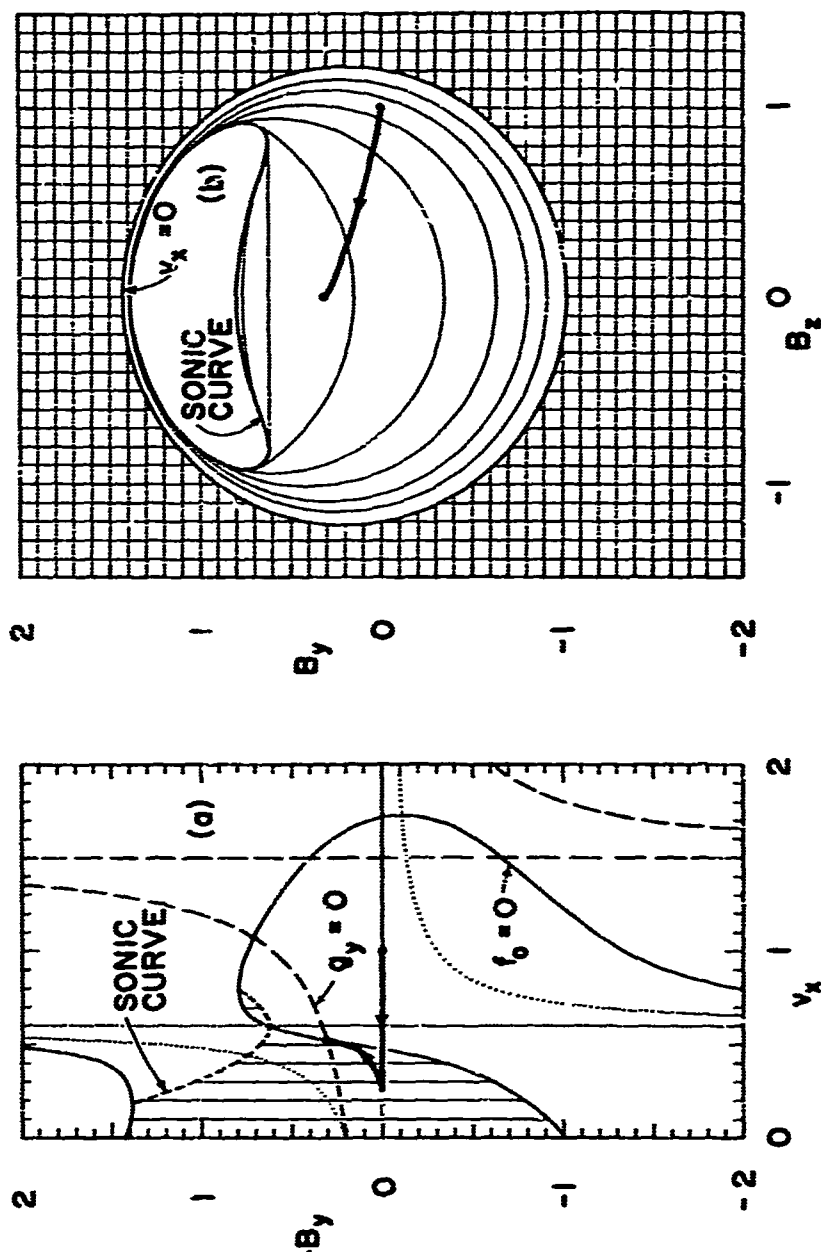layer for the same parameters as in figure 1.

FIGURE 4. Two projections of a structure traject-
ory in (v_x, B_y, B_z) space shown in relation to the
surface $f = 0$, for the case $B_{y1} = 0, B_{z1} = 1$.

mirror-image solution for the same B_{z1} and a corresponding negative value of E_z with the same magnitude. [This is also true in the case of normal shocks (which also have $B_{y1} = 0$); but in these cases, $B_{z1}=0$ in addition, and the structures are plane-polarized.]

In order to consider the full ranges of the parameters governing skew shock magnetic field angles, the above discussion implies that projections of upstream points need be taken only in the first quadrant of the (B_y, B_z) plane, assuming that $B_{y2} \neq 0$. [B_{y2} may vary over a range of positive and negative values, depending on the value of E^*.] Upstream points with projections on the B_y axis correspond to oblique shocks, with the origin representing normal (possibly switch-on) shocks. With upstream projections on the B_z axis, only strictly positive values of B_{y2} (corresponding to $E_z > 0$) need be considered. I all cases, switch-off shocks, $B_{y2} = 0$, can be treated as oblique shocks by reorientation of the coordinate system.

In considering typical examples of skew shocks, the remainder of this paper will be concerned only with the single set of upstream angle conditions: $B_{y1} = 1$, $B_{z1} = 1$, since, clearly, the large number of input parameters $(\gamma, M_1, B_{y1}, B_{z1}, \alpha_{x1}^2,$ and $E_z)$ makes more complete cataloguing out of the question.

3.2 Variation with E^*

If different values of E^* are taken, holding the other parameters constant the various resulting hyperbolas, $g_y = g_z = 0$, are qualitatively easily visualized; however, the shape of the curve $f_o = 0$ changes considerabley with E^*. It is therefore

more convenient to plot a new curve in the (v_x, B_y) plane which is independent of E^*, giving the <u>locus</u> <u>of</u> <u>downstream</u> <u>points</u> (together with other extraneous intersections of $g_y = 0$ with $f_0 = 0$) as E^* is varied parametrically, for constant values of the other parameters. This is obtained by eliminating E^* and $B_{y\text{£}}$ between equations (46), (47), and (30), giving

$$h(v_x, B_y) = (B_y - B_{y1})\left\{B_y - \frac{[(\gamma-1)\alpha_{x1}^2 - \gamma v_x]B_{y1}}{[(\gamma-1)\alpha_{x1}^2 + (2-\gamma)v_x]}\right\}$$

$$- \frac{[(\gamma-1)\alpha_{x1}^2 - \gamma v_x]B_{z1}^2}{[(\gamma-1)\alpha_{x1}^2 + (2-\gamma)v_x]}$$

$$+ \frac{(\gamma+1)(v_x - 1)(v_x - v_x^*)}{\alpha_{x1}^2[(\gamma-1)\alpha_{x1}^2 + (2-\gamma)v_x]}$$

$$= 0. \tag{48}$$

The intersection of this <u>oval</u> curve with the downstream - singular - point hyperbola of equation (46) for a given value of E^* gives the possible location of the downstream point in the (v_x, B_y) plane, provided certain structural and thermodynamic requirements are met. This is shown in figure 5: $\gamma = 5/3$, $M_1 = \infty$, $B_{y1} = 1$, $B_{z1} = 1$, and $\alpha_{x1}^2 = 1.5$, for several values of E^*. The respective projections of the magnetic trajectories are also shown. It is clear from figure 5(a) that there is a maximum[†] and a minimum

---

[†] See § 3.3 for a case in which the maximum E^* value is limited by the saddle-point-separatrix solution.
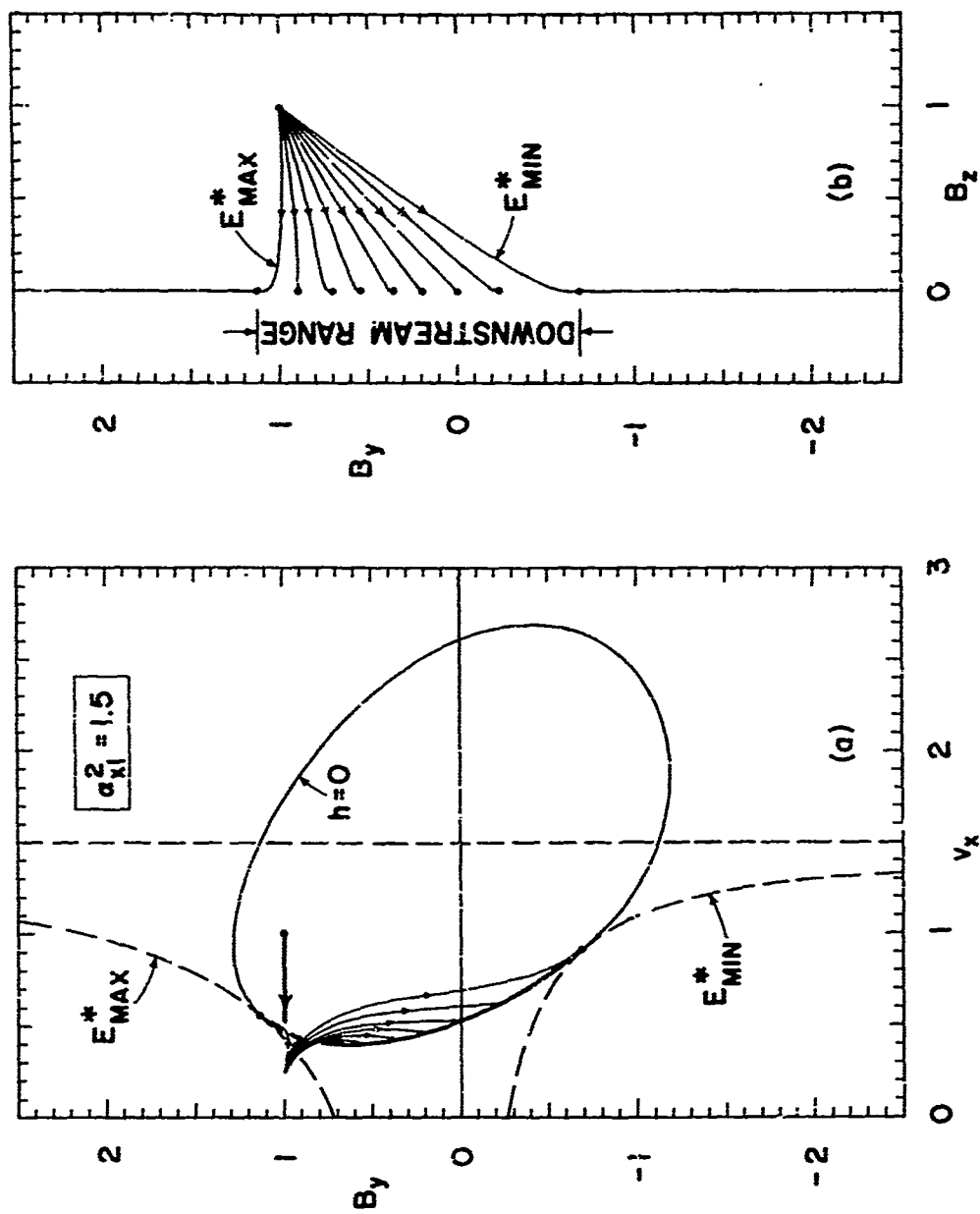
FIGURE 5. Range of downstream states shown by the heavy curve on h = 0. Typical trajectory projections are shown for values of E^* throughout the range.

value of E^*, in between which solutions may exist (shown by the heavy curve on a section of $h = 0$), provided they also satisfy the thermodynamic requirements; e.g., negative temperature (or pressure) obviously must not occur on a structure trajectory. Outside of this range of E^*, no solutions are structurally possible. The type of downstream points corresponding to $E^* = E^*_{MAX}$ or E^*_{MIN}, where the hyperbola $g = 0$ is tangent to the curve $h = 0$, have sometimes been referred to as (generalized) Chapman - Jouguet points, because the downstream normal velocity is just equal to the downstream magneto-acoustic speed in these cases [see Kunkel and Gross (1962)].

In order to get some idea of the temperature variation in the magnetic layer, it is necessary to visualize the intersection of a structure trajectory with the family of lamellar surfaces of revolution about the v_x axis, given by $\hat{T} = $ const. from equation (38)[†]. In the infinite-Mach-number case, this equation becomes

$$\tfrac{1}{2} \frac{(\gamma + 1)^2}{(\gamma - 1)} v_x [1 - v_x - \tfrac{1}{2}\alpha^2_{x1}(B^2_r - B^2_{r1})] = \hat{T}. \tag{49}$$

The intersection of these surfaces with the (v_x, B_y) plane is shown in figure 6, which also includes the downstream locus curve, $h = 0$, the limiting hyperbolas, and a trajectory projection

---

[†]Note that this equation is also independent of E^*.
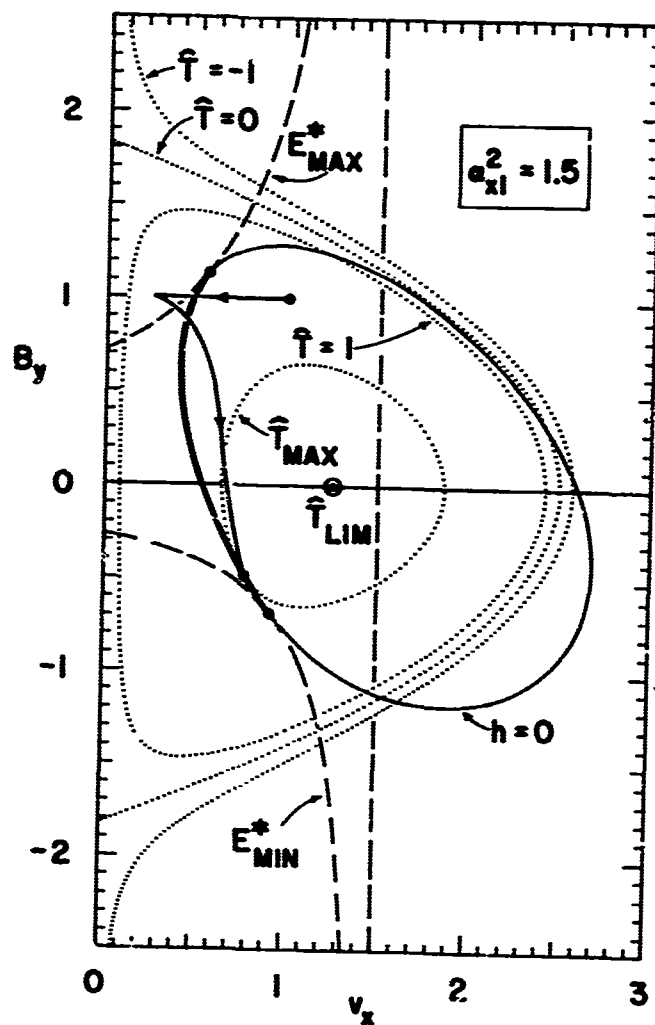
FIGURE 6. Constant-temperature surfaces of
revolution shown by their intersection with
the (v_x, B_y) plane (dotted curves), in relation
to the downstream locus h=0, and the limit-
ing hyperbolas.

corresponding to the E^* value (= E^*_{HOT}, say) for which $\hat{T}_2(E^*)$ has its maximum value $\hat{T}_{MAX}$ for this set of the other parameters. In addition to section curves for the surface $\hat{T} = 0$ (which contains the upstream point) and for the surface $\hat{T} = 1$ (which contains the downstream subshock point), section curves are also given for the surfaces $\hat{T} = -1$, for reference, and $\hat{T} = \hat{T}_{MAX}$. The latter is clearly given by that value of $\hat{T}$ for which the section curve is tangent to $h = 0$ in the range where structures are possible.

Typically, figure 6 shows that the structurally - allowable range on $h = 0$ lies well inside the $\hat{T} = 0$ section - curve parablola, and that all the trajectories lie inside the correspending paraboloid of revolution. On a trajectory, $\hat{T}$ jumps from 0 to 1 across the subshock, and then varies continuously towards its downstream equilibrium value (although not necessarily monotonically).

Note that the parabola for $\hat{T} = 0$ intersects the v_x axis at $v_{xo} = 1 + \frac{1}{2}\alpha^2_{x1}B^2_{r1}$, and the corresponding paraboloid meets the (B_y, B_z) plane at $B^2_r = B^2_{r1} + 2/\alpha^2_{x1}$. For reference, the point corresponding to the limiting (maximum) value of $\hat{T}$ for which there are real surfaces, $\hat{T}_{LIM}$, has also been shown. This occurs on the v_x axis at $v_x = \frac{1}{2}v_{xo}$, giving the value $\hat{T}_{LIM} = \frac{1}{8}(\gamma+1)^2 v^2_{xo}/(\gamma-1)$. In general, $\hat{T}_{MAX}$ (which must occur on $h = 0$) will be less than $\hat{T}_{LIM}$.

It has been found that $\hat{T}_{MAX}$ usually occurs at points having values of B_{y2} near zero. By inspection of equation (49), it is

clear that this corresponds to most of the magnetic energy having been converted into thermal energy (through Joule dissipation). The fact that B_{y2} is not exactly zero for $\hat{T}_{MAX}$ is due to the coupling with the flow kinetic energy through the v_x terms in equation (49).

In skew shocks in which $B_{z1} = \underline{0}(1)$, $\underline{all}$ $\hat{T}_2$ values are usually greater than the viscous temperature $\hat{T} = 1$, because the transverse magnetic field magnitude has <u>decreased</u>, thus creating thermal energy downstream. However, in some cases (especially for oblique or almost - oblique shocks operating near the <u>upper</u> Chapman - Jouguet point), the transverse magnitude may actually increase, and $\hat{T}_2$ will be slightly <u>less</u> than the viscous temperature. Thus in shock - tube experiments operating in the Chapman - Jouguet mode, if one of the goals is the achievement of high downstream temperatures by making use of the "magnetic dumping" effect of Joule heating, it is clearly desirable to try to produce the <u>lower</u> Chapman - Jouguet condition rather than the upper one.

3.3 <u>Variation with</u> α_{x1}^2

For other values of α_{x1}^2, the behaviour is qualitatively similar to the case for $\alpha_{x1}^2 = 1.5$, given above, over a finite range of α_{x1}^2. As the magnetic pressure ratio is increased, the oval curve of figure 5 at first elongates in the v_x direction and shrinks in the B_y direction, bodily moving towards larger v_x values. At higher α_{x1}^2 values, it shrinks in its

v_x dimension as well. For all skew shocks, there is an upper limit on α_{x1}^2 at which this oval curve disappears entirely (for oblique and normal shocks, there is no upper limit). However, well before this limit is reached, certain structural properties limit the range of E^* values to lie in a restricted range, not extending to one or both of the tangent points (i.e., one or both of the Chapman-Jouguet points are excluded). This is because the topology of the surface $f = 0$ is such that, for E^* values outside of the restricted range, the trajectory passing through the subshock point, instead of travelling on the subsonic sheet directly to the nodal singularity, runs into the sonic curve, at which point it must leave the surface, flying off to $v_x = \infty$. [This phenomenon shows up in the numerical integrations as v_x becoming imaginary in the subsequent increment in x.]

Figure 7 shows a set of trajectories for $\alpha_{x1}^2 = 2.3$. The maximum E^* value is <u>not</u> restricted to lie below the tangent (Chapman-Jouguet) value, and the behaviour is similar to that of smaller magnetic pressure ratios until E^* reaches a value near -0.33 (compared with the <u>lower tangent</u> value of -0.444). Figure 8 shows why lower E^* values are impossible.

Note in figure 7 the occurrence of overall expansion shocks. After the sudden gasdynamic compression through the viscous subshock, MHD interaction expands the gas, as magnetic energy is converted into directed kinetic energy. The density profile and corresponding magnetic field, temperature, and entropy plots are shown in figure 9. It should be noted that these expansion
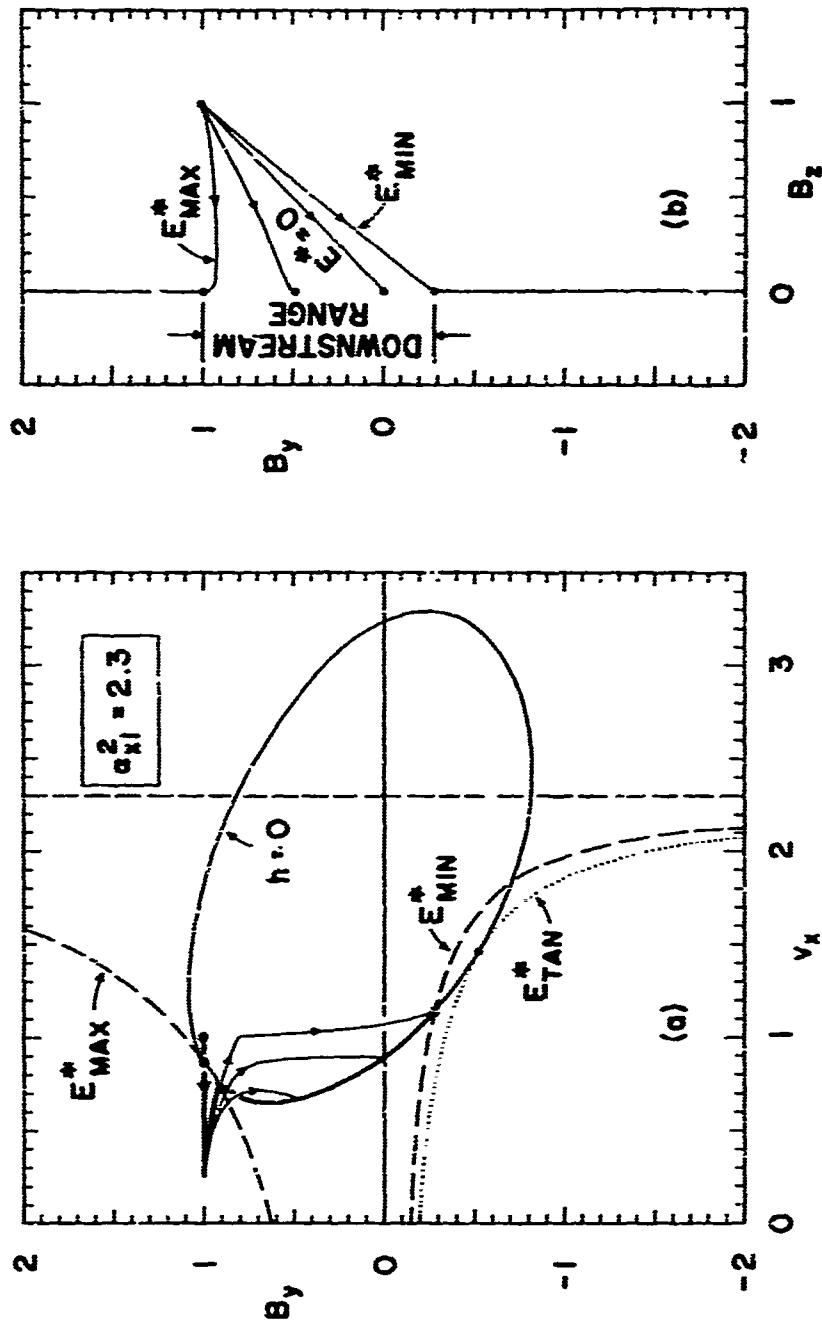
FIGURE 7. Downstream locus curve and trajectory projections for E^* within the allowable range. In this case, E^*_{MIN} lies above the tangent value because of structural restrictions.
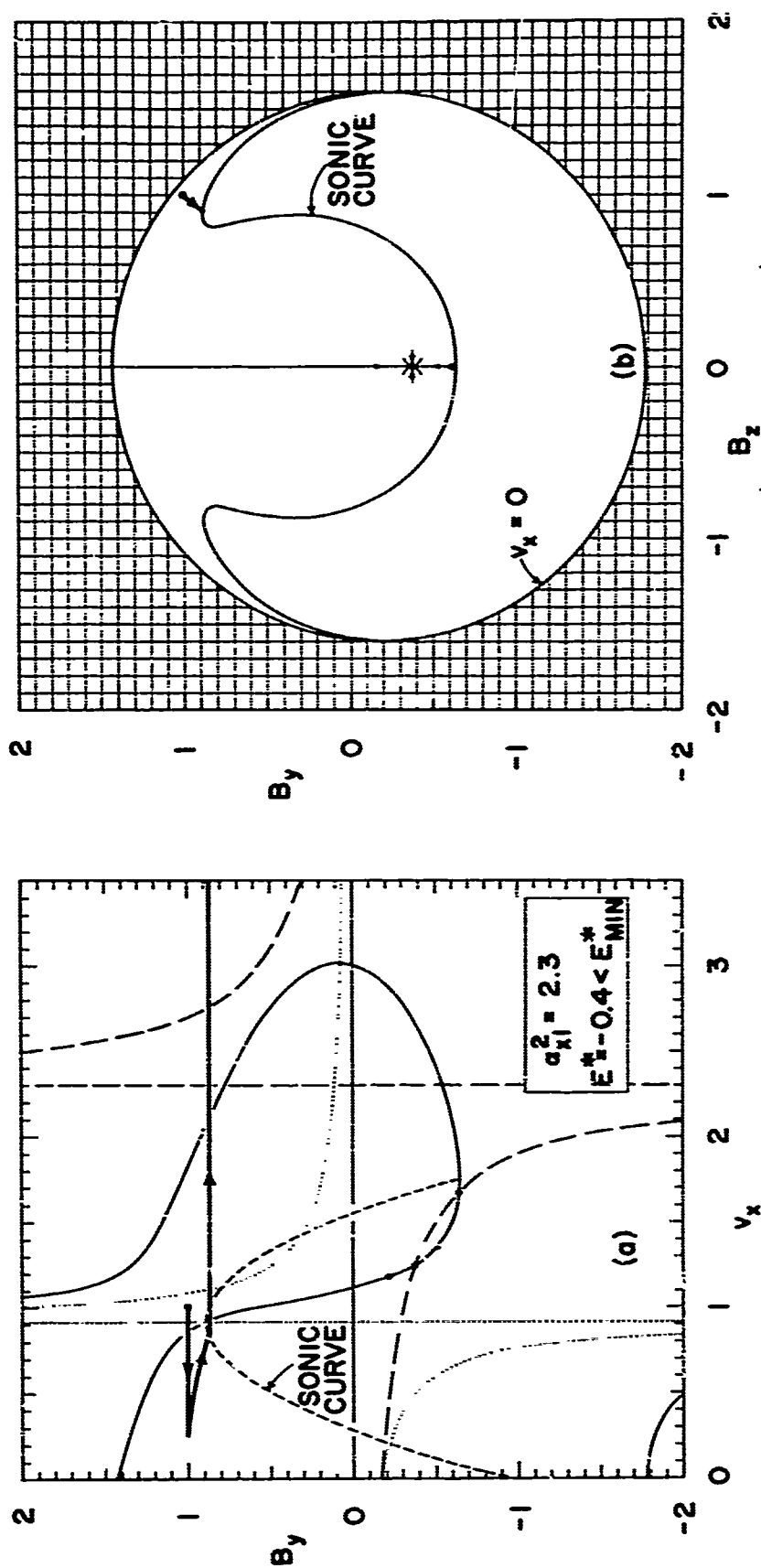
FIGURE 8. Physically-unacceptable trajectory for E^* between E^*_{MIN} and E^*_{TAN}. On the sonic curve the entropy is stationary, and trajectories either leave (entropy maxima) or approach (entropy minima) the surface tangentially along straight lines parallel to the v_x axis.
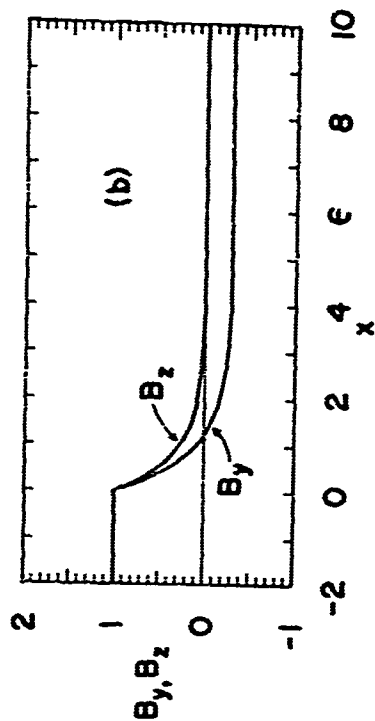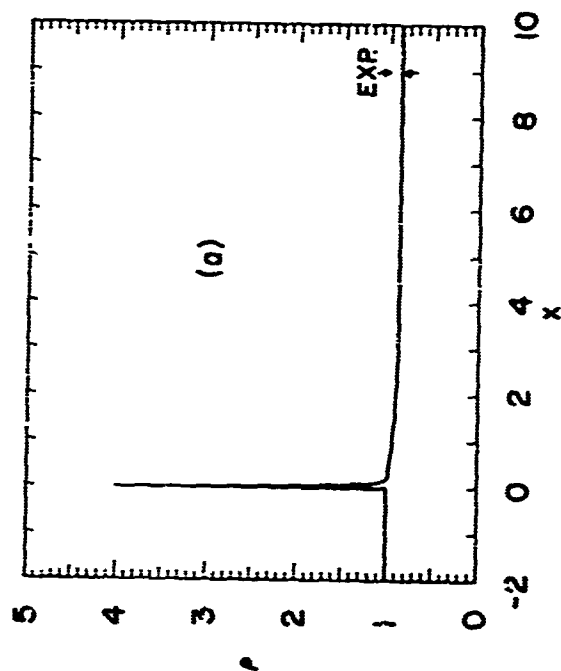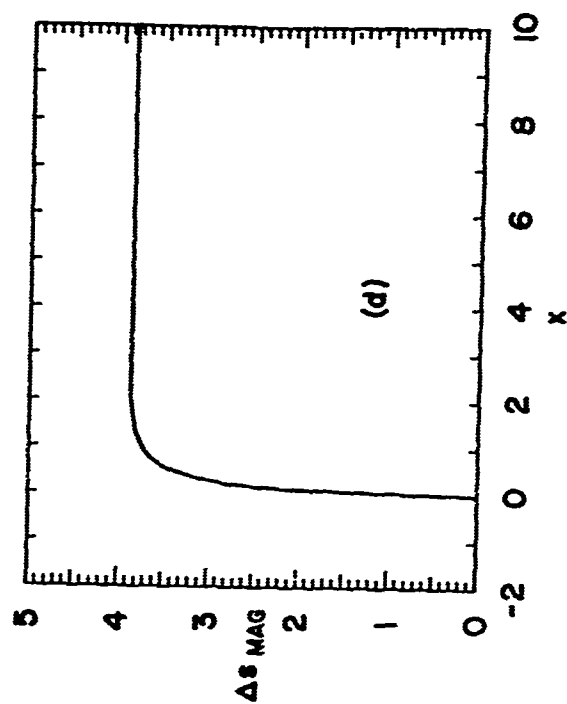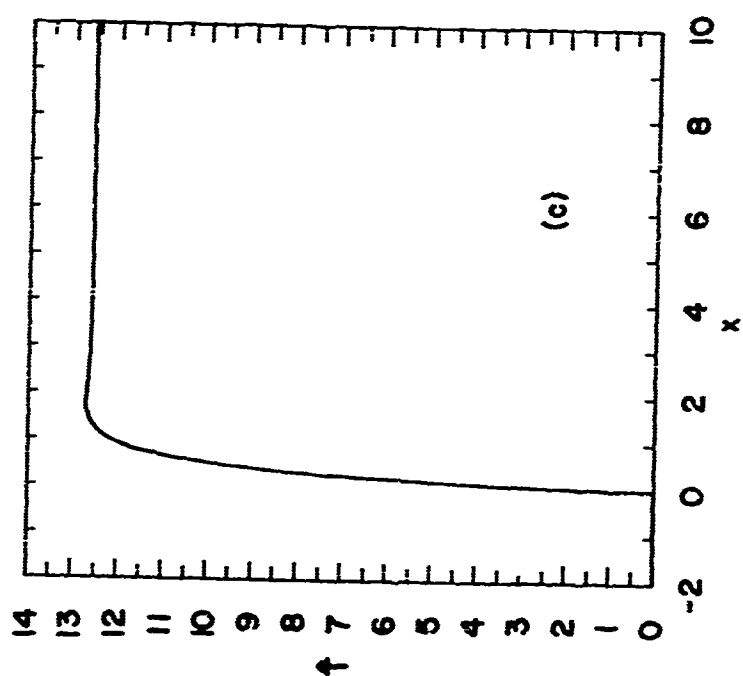
FIGURE 9. Structure profiles for the overall-expansion shock corresponding to E^*_{MIN} of figure 7.

shocks also develop relatively large downstream temperatures due to Joule heating. In such cases, it is evident that the expansion is not at the expense of thermal energy.

At still larger values of α_{x1}^2, there is a restriction on the maximum E^* value as well, as shown in figure 10 for $\alpha_{x1}^2 = 2.9$. There are no solutions above $\alpha_{x1}^2 = 2.92$.

Structural restrictions of a different nature occur at values of α_{x1}^2 numerically near v_x^* ($= 0.25$ in this infinite-Mach-number case). This concerns the relative position of the separatrix going into the saddle point which occurs on the subsonic sheet of $f = 0$ for these smaller values of α_{x1}^2. In some cases, the upper tangent value of E^* is such that this separatrix does not enclose the subshock point, as shown in figure 11(a) for $\alpha_{x1}^2 = 0.27$, and E_{MAX}^* is restricted to a smaller value, as shown in figure 11(b). Structures of this latter limiting type are actually composed of two shocks: a skew shock (including the viscous subshock) leading to conditions given by the saddle-point singularity, followed (at an arbitrary distance downstream) by a slow, completely subsonic, MHD oblique shock from the saddle point to the nodal singularity. The isolated saddle-point solution is the analogue of the (magnetically trivial) gas shock appearing in the case of purely oblique ionizing shock structures which are sub-Alfvénic downstream. [Clearly, there is a unique value of E^* associated with this type of solution — a common feature of all
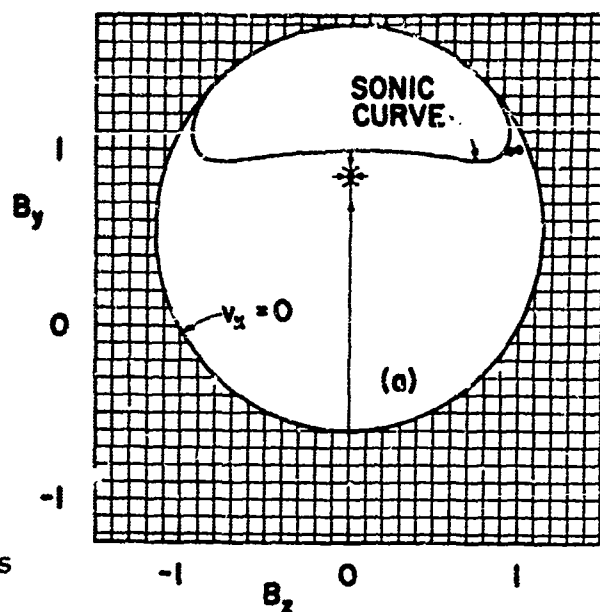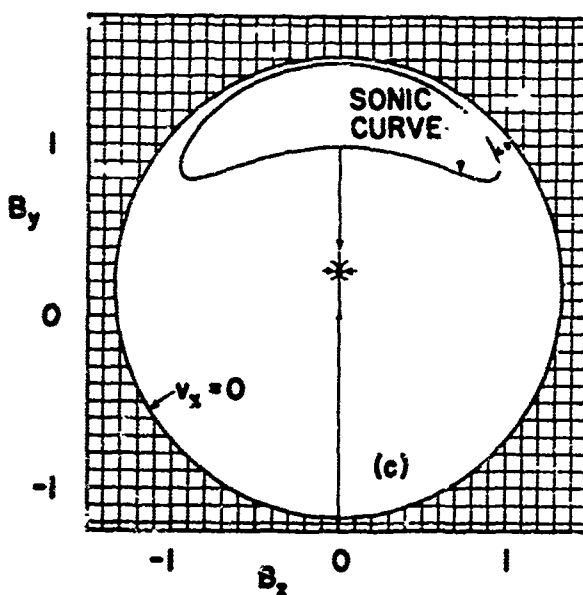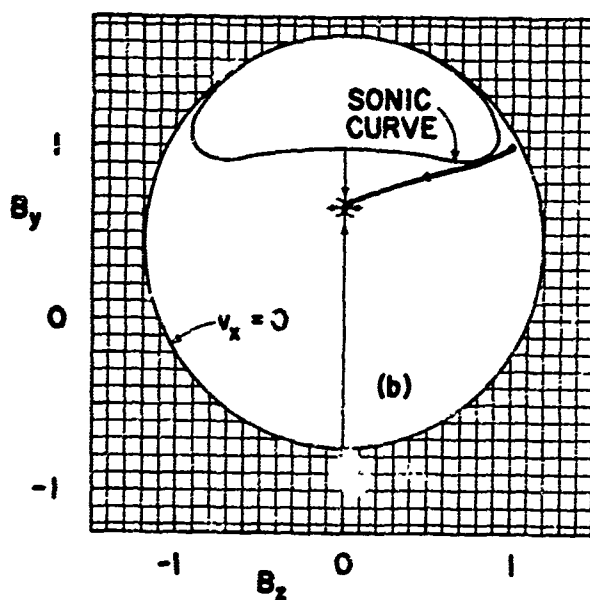
FIGURE 10. Structural restrictions on E_{MAX}^*. In (a), the trajectory runs into the sonic curve because the downstream point is fairly high. In (b), a solution is possible for a smaller E^* value due to the lower downstream point and the fact that the kidney-shaped sonic curve projection has not extended very far. In (c), for a smaller E^* value, although the downstream point is still lower, the sonic curve has elongated so far that a solution is not possible. For larger values of α_{x1}^2, conditions (a) and (c) coalesce.

$\alpha^2_{x1} = 0.27$
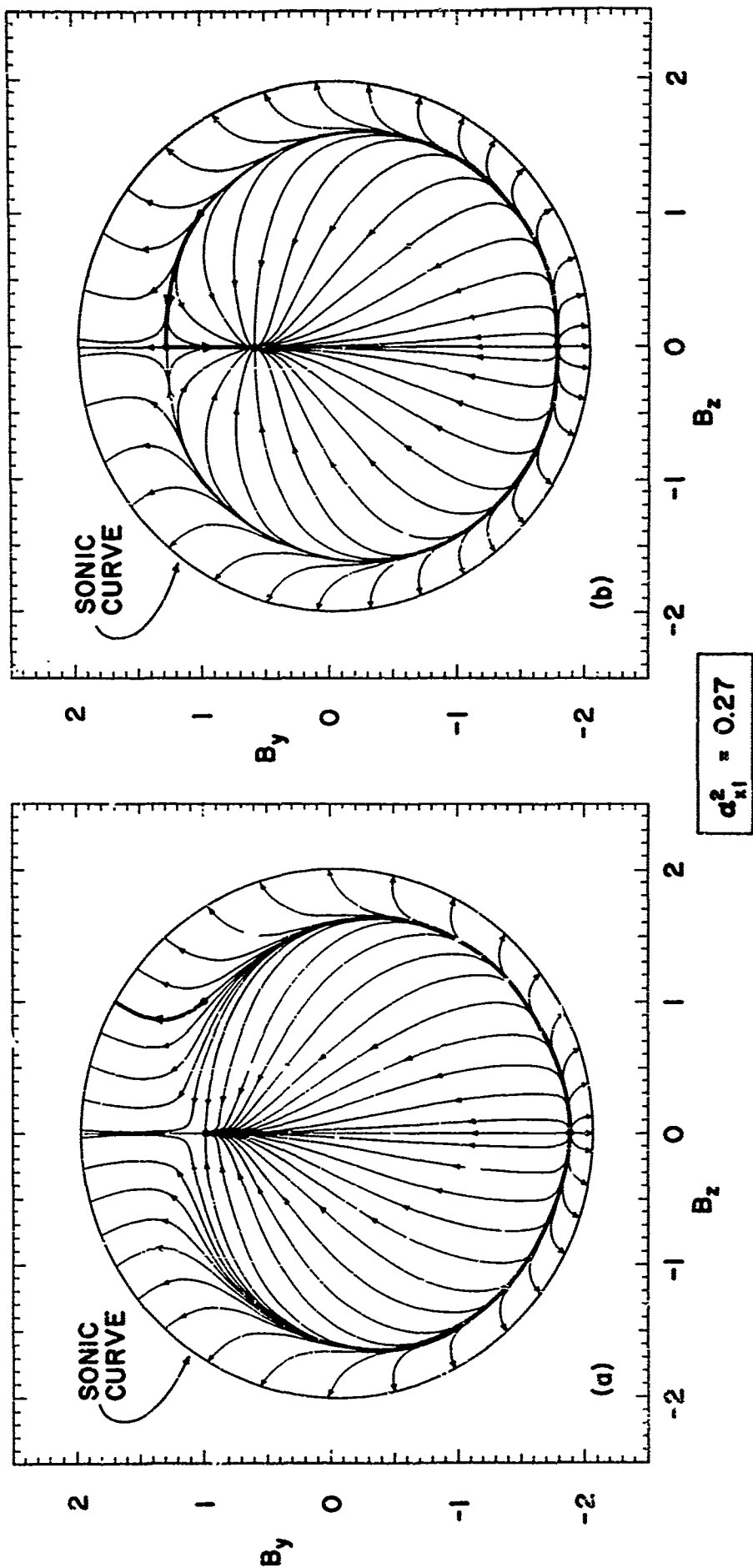
FIGURE 11. Structural restrictions on E^*_{MAX} for α^2_{x1} near v^*_x. In (a), the subshock point lies on an unacceptable trajectory. In (b), $t^* = E^*_{MAX}$; This is the limit solution where the subshock point is on the separatrix.

shock waves involving downstream saddle points.] However, there are no skew shock structures analogous to the super-Alfvénic gas shocks (because skew shocks must always be sub-Alfvénic downstream), and so there is a distinct lower limit to α_{x1}^2 (upper limit to the shock Alfvén number A_1) beyond which skew shocks do not occur, for a given set of upstream field angles.

These properties can be summarized by making graphs of the ranges of E^* and the downstream quantities B_{y2}, v_{x2}, and $\hat{T}_2$, plotted against α_{x1}^2, or, preferably, against A_1 ($= \alpha_{x1}^{-1}$), which gives a direct measure of shock speed. For comparison with earlier work by Taussig (1965, 1967) on normal and oblique shocks, the range of the downstream Alfvén number $A_2 = \overline{v}_{x2}\sqrt{\mu\overline{\rho}_2} / \overline{B}_x = A_1\sqrt{v_{x2}}$ is also plotted against A_1. Figures 12(a)-(e) show these ranges. The details of E^*, v_{x2}, and $\hat{T}_2$ for A_1 near $v_x^{*-\frac{1}{2}}$ are shown on a finer scale in figures 13(a), (b), and (c).

In addition to the Chapman-Jouguet and structurally-limited boundaries in figures 12 and 13 (solid curves), the tangent values are shown (dotted), and also the locus of maximum temperature points (light dashed). The saddle-point solutions are shown by the heavy dashed curve. Expansion shocks occur in the shaded region. Switch-off shocks have $E^* = B_{y2} = 0$.

The plots of v_{x2}, A_2, and $\hat{T}_2$ can be visualized as projections of three-dimensional surfaces, the other coordinate being E^*. In this way, the double-valued regions may, perhaps,
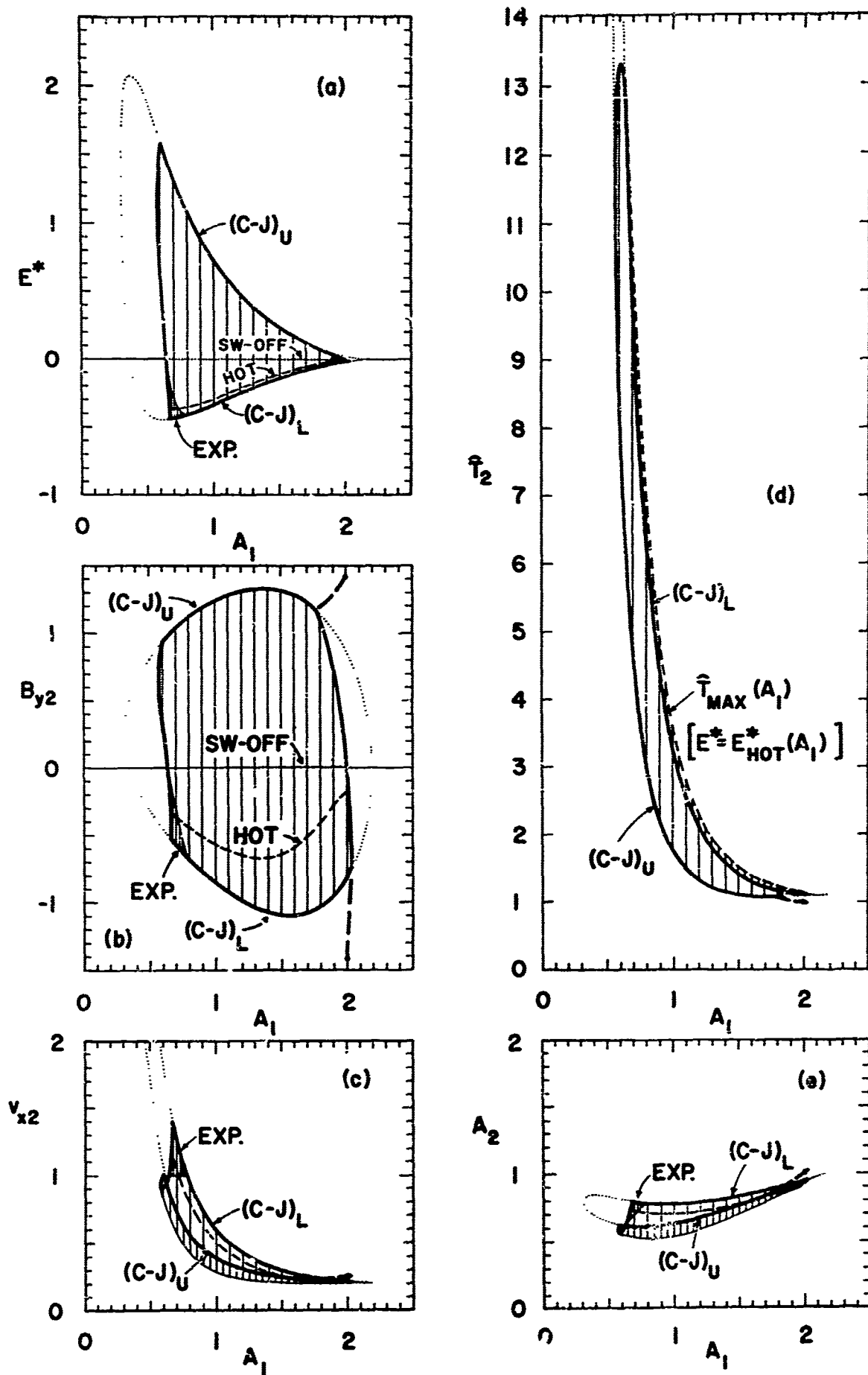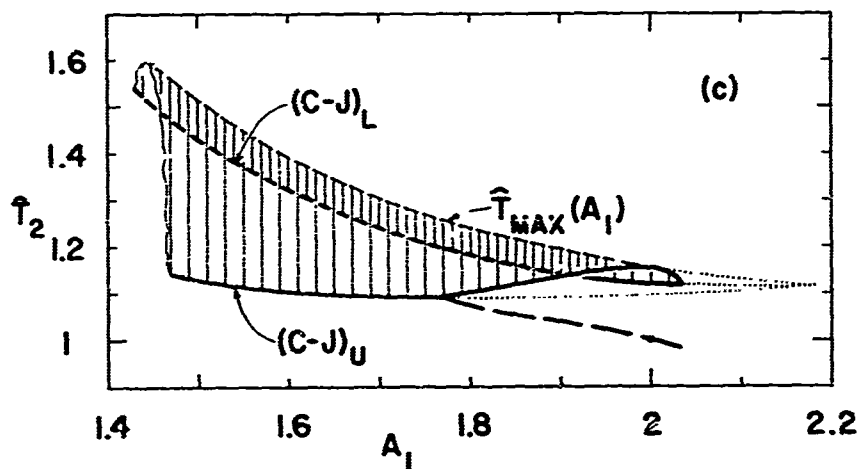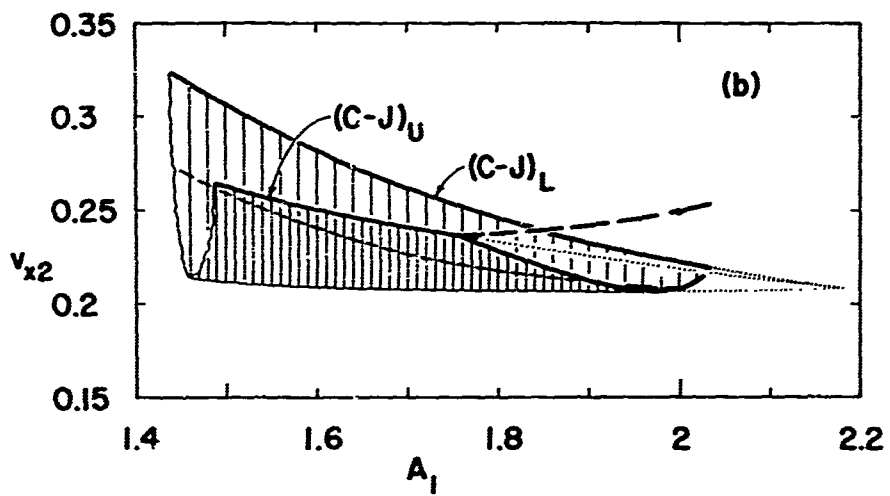
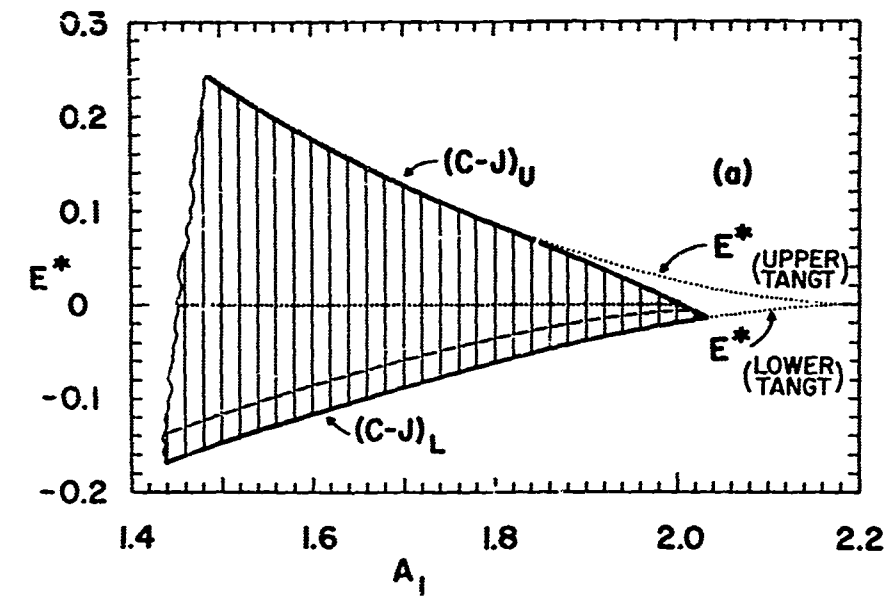FIGURE 12. Allowable ranges of the downstream variables.

FIGURE 13. Detailed behaviour of the allowable-range plots near $A_1 = (v_x^*)^{-\frac{1}{2}}$. The dashed curves show the locus of saddle-point solutions cf. figure 11 (b).

be more readily comprehended.

Finally, it should be noted that, under optimum condi-
tions, significant Joule heating can occur, giving maximum
downstream temperatures up to about 13 times as large as
the viscous subshock temperature, for this particular set of
upstream field angles ($B_{y1} = B_{z1} = 1$). This is because mag-
netic energy has been converted into thermal energy, the effect
becoming rapidly stronger as the magnetic pressure ratio α_{x1}^2
is increased (or Alfvén number A_1 decreased) until struc-
tural limitations are met.

Conclusion

The most general form of ionizing shock wave involves a magnetic field vector whose transverse component may rotate while changing magnitude throughout the shock layer. These are called skew shocks because the upstream and downstream magnetic field vectors and the shock wave normal do not, in general, all lie in a single plane. This phenomenon arises because the electric field in the nonconducting upstream region has a certain amount of freedom in both magnitude and direction. Much has been written previously on the degree (or lack) of freedom of the transverse electric field magnitude in ionizing shock waves. There seems to have been a certain amount of hesitancy in being prepared to assign the electric field the status of a parameter, and many studies have apparently been motivated by an attempt to find conditions requiring a unique value of the E - field. The philosophy of the present approach has been to treat the E - field as a (free) parameter, allowing the detailed structure to determine whether or not there are unique values associated with certain kinds of solution. As is well known in the theory of nonlinear two-point boundary-value problems, parameter-uniqueness is always associated with the requirement of a solution trajectory to lie exactly on a saddle-point separatrix. Thus, in ionizing shock wave theory, those structures which involve a downstream saddle point will be associated with a unique value of the transverse E - field;

i.e., the $\underline{E}$ - field will be structurally determinate. [The downstream singularity is the determining one for ionizing shock waves because upstream, there is no singular point in phase space but, rather, a whole region (lying on $f = 0$) in which $\sigma = 0$.] The saddle point may lie in the (v_x, B_y) plane as is the case for oblique (and normal) ionizing shock waves, or (for $Pm = 0$) on the $f = 0$ surface [as seen, for example, by projection onto the (B_y, B_z) plane] in the case of skew shocks. The former may have structures for super-Alfvénic as well as sub-Alfvénic saddle points, but the latter exist only for sub-Alfvénic saddle points. Transverse shocks always involve a super-Alfvénic downstream saddle point in the (v_x, B_y) plane. In zero-Pm theory, all (v_x, B_y) - saddle-point structures are magnetically trivial gas shocks.

Much more interesting, however, is the range of structures possible when the downstream point is a (necessarily sub-Alfvénic) node. In this case the $\underline{E}$ - field is a free parameter, and can range over a continuum of values between limits determined by other kinds of topological features of the structure. In zero-Pm skew shocks, this node lies in the subsonic sheet of the $f = 0$ surface. [In fact, this singularity (which is characterized by $v_x < c_s$, the slow magneto-acoustic speed) is also nodal in the (v_x, B_y) plane; however, for zero Pm, the form is degenerate, and all trajectories enter along the curve $f_o = 0$, except for one straight line parallel to the v_x axis.]

One difficulty in studying ionizing shock waves is in cataloguing the large number of different types of solutions for ranges of the <u>five</u> governing parameters: Mach number, Alfvén number, two field angles, and the transverse electric field. This analysis has been restricted to $M_1 = \infty$, and most of the solutions are given for $B_{y1} = B_{z1} = 1$; thus, A_1 and E_z (actually, $E^* = E_z + A_1^{-2} B_{y1}$) are the main parameters of interest.

Finally, it should be stressed that this analysis has studied the <u>magnetic</u> structure of skew shocks. This is made possible by the coordinate transformation of § 2.3, which decouples variable ionization and nonequilibrium electron temperature effects on the electrical conductivity. The structure of these variables can now be studied separately, with the known magnetic structure being used as an input (through Joule heating and the MHD interaction on the fluid variables). The two classes of problem are finally combined by making the inverse coordinate transformation (a single straight-forward numerical integration). Work is proceeding along these lines.

Acknowledgements

Appendix

<p style="text-align: center;">Integral curves on   f = 0</p>

The shape of the surface $f = 0$ is defined by a family
of circles v_x = const., whose centres lie on the centreline
hyperbola: $B_y = B_{y\xi}(v_x)$, $B_z = 0$.   The intersection of the
surface with the (v_x, B_y) plane forms the curve $f_o = 0$,
the detailed shape of which varies considerably depending on
the value of E^*, and the location of the asymptote of the
centreline hyperbola, $v_x^A = (\gamma-1)\alpha_{x1}^2 / \gamma$, relative to $v_x = v_x^*$
and $v_x = 1$.

There are so many topologically different characteristic
shapes, that it is not feasible to indicate all of them here.
Instead, a few cases will be chosen which most clearly demon-
strate the qualitative behaviour of the integral curves lying
on $f = 0$.

This surface can be considered to be divided into two
"sheets" by the space curve lying on it formed by the locus
of points of tangency of lines parallel to the v_x axis.   Since
grad f   [in (v_x, B_y, B_z) space] must be perpendicular to the
v_x axis on this curve, it is given by the intersection of $f = 0$
with the surface

$$\left(\frac{\partial f}{\partial v_x}\right)_{B_y, B_z} = \frac{2}{(\gamma-1)}\left(1 - \frac{1}{M^2}\right) = 0 , \qquad (A.1)$$

from equations (29), (30), (31), and (33), where M is the
local Mach number, given by

$$M^2 \;=\; \frac{\bar{v}_x^2}{\bar{a}^2} \;=\; \frac{v_x^2 \, \bar{v}_{x1}^2}{T \, \bar{a}_1^2} \;=\; M_1^2 \left(\frac{v_x^2}{T}\right) , \qquad (A.2)$$

since the ordinary sound speed $\bar{a}$ is proportional to $\bar{T}^{\frac{1}{2}}$.
It can be shown that M is a monotonically increasing function
of v_x, for a fixed $|\underset{\sim}{B}|$, thus the two sheets of f = 0 can
be labelled as "supersonic" (corresponding to larger v_x values)
and "subsonic", being sparated by the "sonic curve", on which
M = 1. As with ordinary gas shocks, an acceptable viscous sub-
shock trajectory must have its upstream end or the supersonic
sheet and its downstream end on the subsonic sheet. The sub-
sequent magnetic portion of the trajectory must, if it is to
be a solution trajectory, lie entirely on the subsonic sheet,
because trajectories on f = 0 which reach the sonic curve
subsequently fly-off to v_x = +∞. This behaviour is similar
to that of slow oblique shocks in a pre-ionized gas [especially
in cases of tensor conductivity (Leonard, 1966)], which always
have their magnetic trajectories on the subsonic sheet of
f = 0, even when there is no subshock ($M_1 \leq 1$). Fast oblique
or normal shocks, however, have their magnetic structure on the
supersonic sheet, upstream (where $\bar{\sigma}_1 \neq 0$) of a subshock, if
one exists.

Figure A.1 represents the case: $\gamma = 5/3$, $M_1 = \infty$,

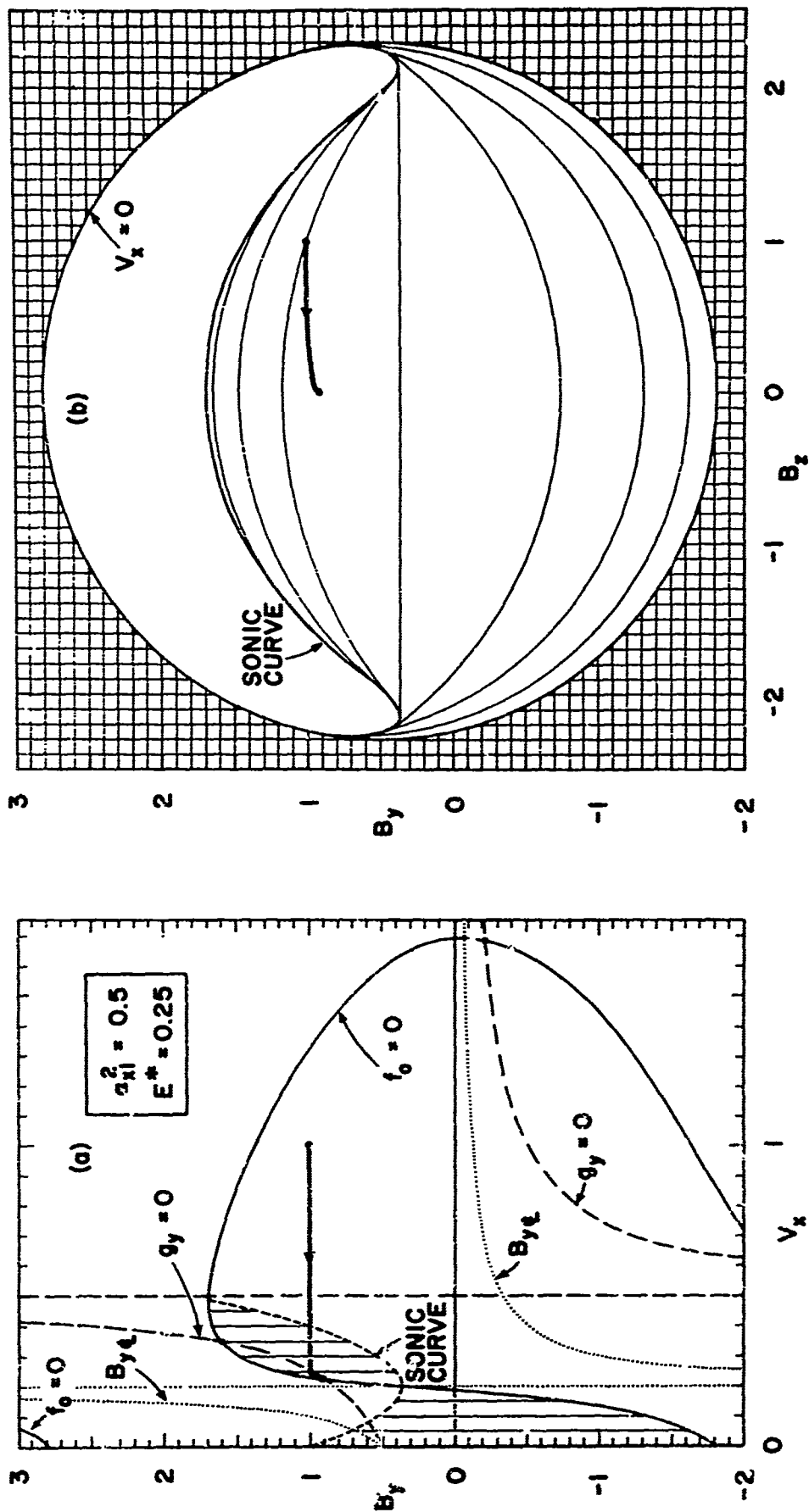FIGURE A.1. Representation of the surface $f = 0$ by projection of section curves v_x = const. on the subsonic sheet. In (a), these are straight lines terminating on $f_0 = 0$ and the sonic curve. In (b), they are circular arcs terminating tangentially at the sonic curve. Projections of the solution trajectory are also shown.

$B_{y1} = 1$, $B_{z1} = 1$, $\alpha_{x1}^2 = 0.5$, $E^* = 0.25$. [For $M_1 = \infty$ and $\gamma = 5/3$, equation (A.2) is written $M^2 = 16v_x^2 / (5\hat{T})$.] In the (v_x, B_y) projection of figure A.1(a), the curve $f_o = 0$ is shown, together with the downstream hyperbola $g_y = 0$ and the centreline hyperbola $B_y = B_{y\ell}(v_x)$. The arrow directions on $f_o = 0$ correspond to the sign of g_y in the three different regions determined by the branches of the downstream hyperbola. Since $g_z = 0$ in the (v_x, B_y) plane, this determines those integral curves which lie in this plane. In figure A.1(b), the circles $v_x = $ const. on the <u>subsonic</u> sheet of $f = 0$ are shown; i.e., this represents the view as seen from the origin, looking in the positive v_x direction.

To find the shape of the remaining integral curves which lie on the subsonic sheet, it is convenient to study their direction-field projection in the (B_y, B_z) plane. From equations (39) and (40), it is seen that

$$\frac{dB_y}{dB_z} = \frac{g_y}{g_z}$$

$$= -\frac{[E^* - (\alpha_{x1}^2 - v_x)B_y]}{(\alpha_{x1}^2 - v_x)B_z}$$

$$= \frac{[B_y - E^* / (\alpha_{x1}^2 - v_x)]}{B_z} . \tag{A.3}$$

Note from this equation that if $v_x = $ const. [a circle in

figure A.1(b)], a given value of $dB_y / dB_z = S$, say, gives

the straight line $B_y - E^* / (\alpha_{x1}^2 - v_x) = SB_z$, which itself has

slope S. Where this straight line intersects the circle

$v_x = $ const., the integral curves at those points have slope S.

In other words, at any point $(v_x^{(f)}, B_y^{(f)}, B_z^{(f)})$ on the sur-

face $f = 0$, the (B_y, B_z) projection of the integral curve

passing through that point is directed along a straight line

joining the point $(B_y^{(f)}, B_z^{(f)})$ with the point $(B_y^{(g)}, B_z^{(g)})$,

where $B_y^{(g)} = E^* / (\alpha_{x1}^2 - v_x^{(f)})$, and $B_z^{(g)} = 0$. The sense of

the arrows representing $dx > 0$ is determined by $d|B_z| / dx \gtrless 0$

as $(\alpha_{x1}^2 - v_x^{(f)}) \gtrless 0$ [or by continuity, on the circle $v_x^{(f)} =$

α_{x1}^2], and by $dB_y / dx \gtrless 0$ as $g_y \gtrless 0$, if $B_z = 0$ [as with

oblique and normal shocks]. To make this clearer, figure A.2

shows four cases depending on the location of the "fan point"

$(B_y^{(g)}, 0)$:

     (a)   inside the circle,

     (b)   on the circle,

     (c)   outside the circle, and

     (d)   at infinity $(v_x^{(f)} = \alpha_{x1}^2)$.

[The sense of the arrows has been assigned arbitrarily.]

Given only the curve $f_o = 0$, it is a very straight-for-

ward matter to make a graphical construction of the complete

direction field, from which the integral curves can be deter-

mined, as shown in figure A.3(b); the (v_x, B_y) projection of

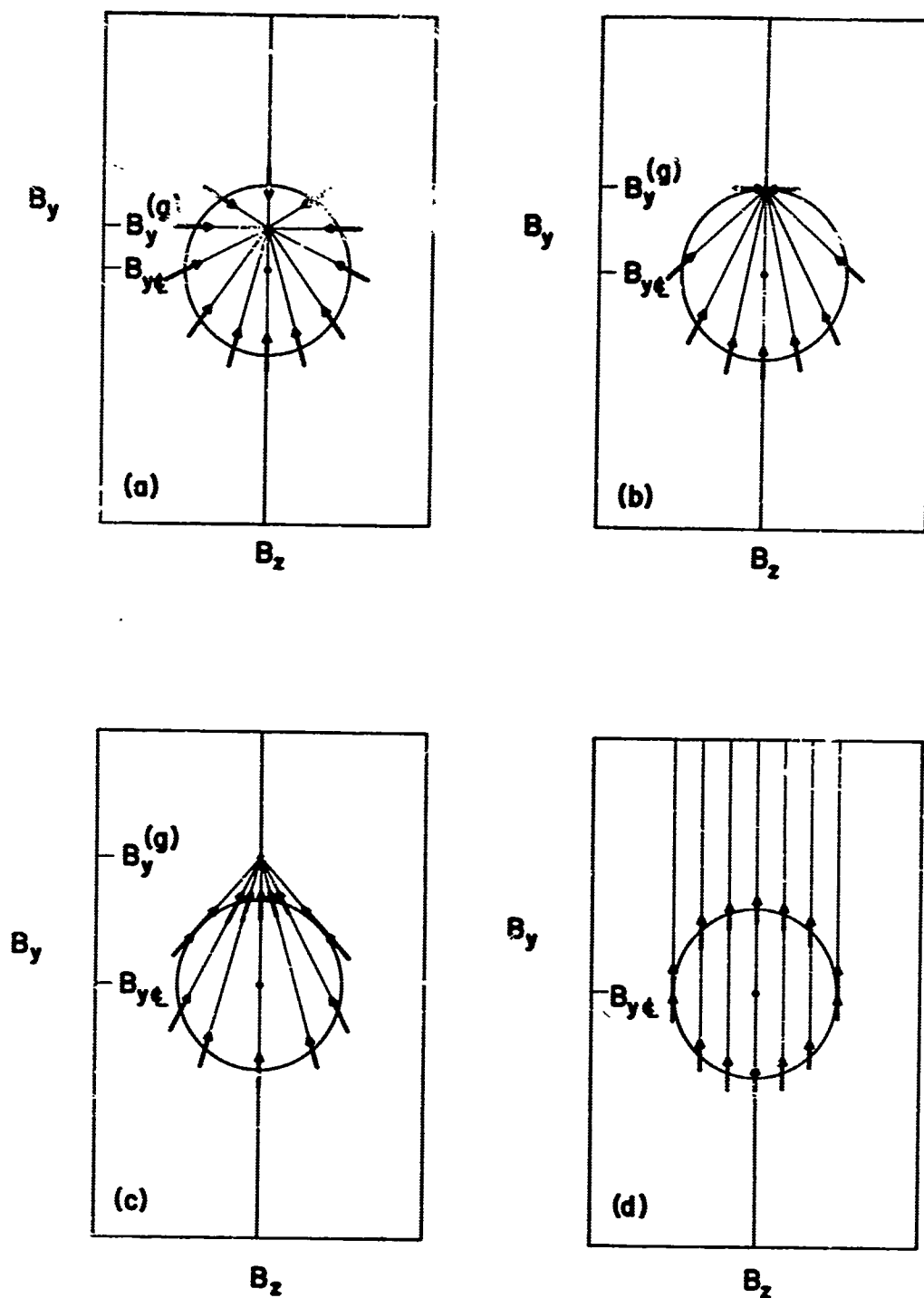figure A.3(a) is found by cross-plotting.

FIGURE A.2. Graphical construction of the direction field projection in the (B_y, B_z) plane.
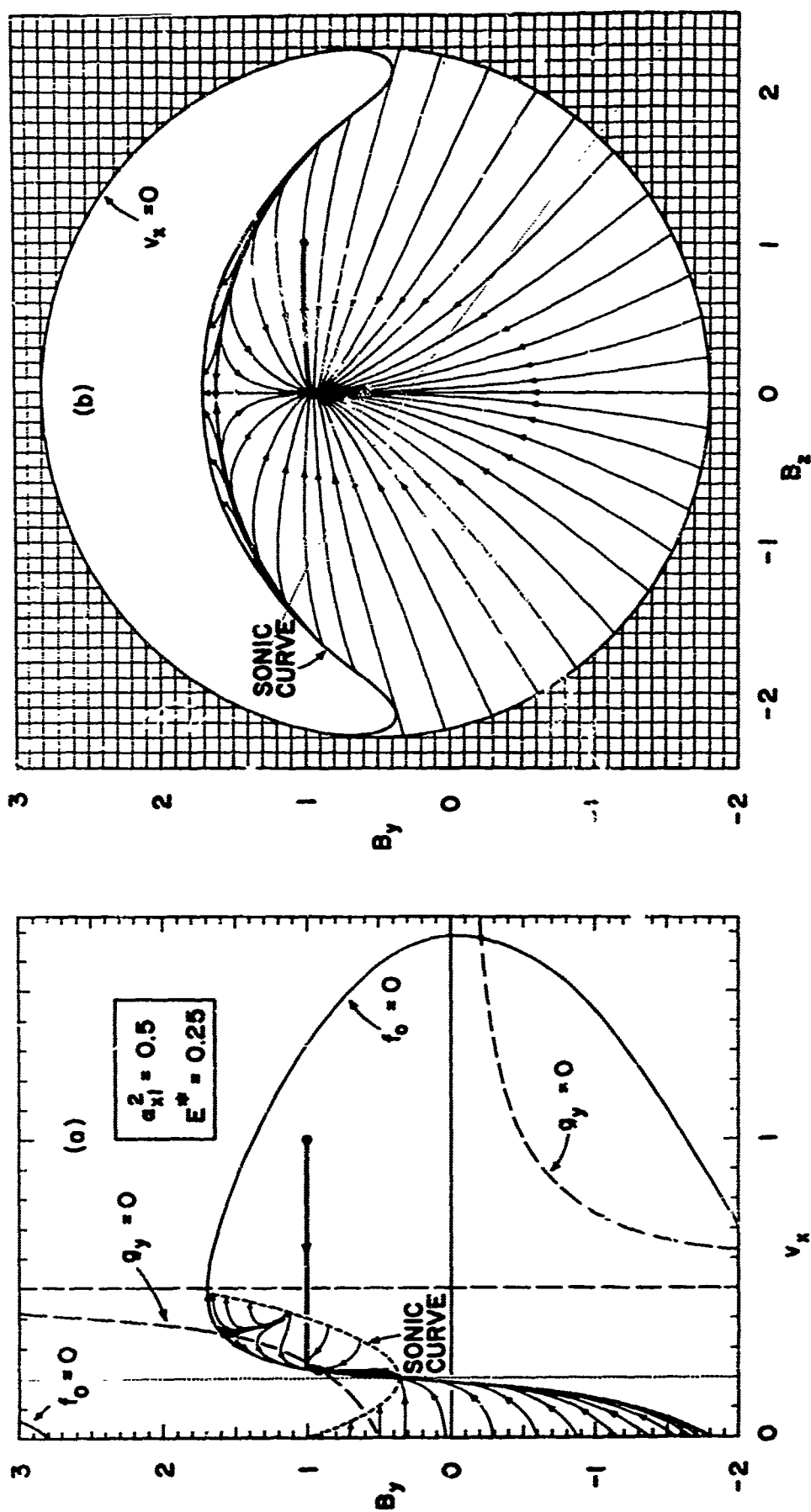
FIGURE A.3. Projections of the subsonic magnetic trajectories for the same case as in figure A.1.

Note that the downstream point is a <u>node</u>, whereas the other intersection of $g_y = 0$ with $f_o = 0$ is a <u>saddle point</u>. The respective separatrices have been shown in slightly heavier curves.

For given upstream conditions [in the present case, the point $(1, 1, 1)$] the <u>solution</u> trajectory jumps from the supersonic sheet to the subsonic sheet at $(v_x^*, 1, 1)$, from which point on it follows the integral curve passing through that point until it reaches the downstream singularity. Note that if $B_{z1} = 0$ (oblique or normal shocks), the complete trajectory lies entirely in the (v_x, B_y) plane, the magnetic portion following $f_o = 0$, which in this case passes through the point $(v_x^*, 1, 0)$. Also, if $E^* = 0$, the surface $f = 0$ becomes a surface of revolution, and all trajectories are radial lines, as shown in figure A.4. Clearly, there is no distinction between oblique and skew shocks in this case; i.e., all switch-off shocks with the same $|\underline{B}_1|$ are plane-polarized, and have identical $|\underline{B}|$ − structure. The downstream singularity in this case is a special type of completely symmetrical node ("sink"); for small $|E^*|$ values, the singularity has the more standard form of figure A.3(b) locally, although, further away from the node, most of the trajectories are fairly straight in (B_y, B_z) − projection.

Finally, figure A.5 shows the case for $\alpha_{x1}^2 = 0.5$, $E^* = E_{MAX}^* = 0.2976$. This is typical of the upper Chapman-Jouguet solutions for moderate values of α_{x1}^2. The singularity
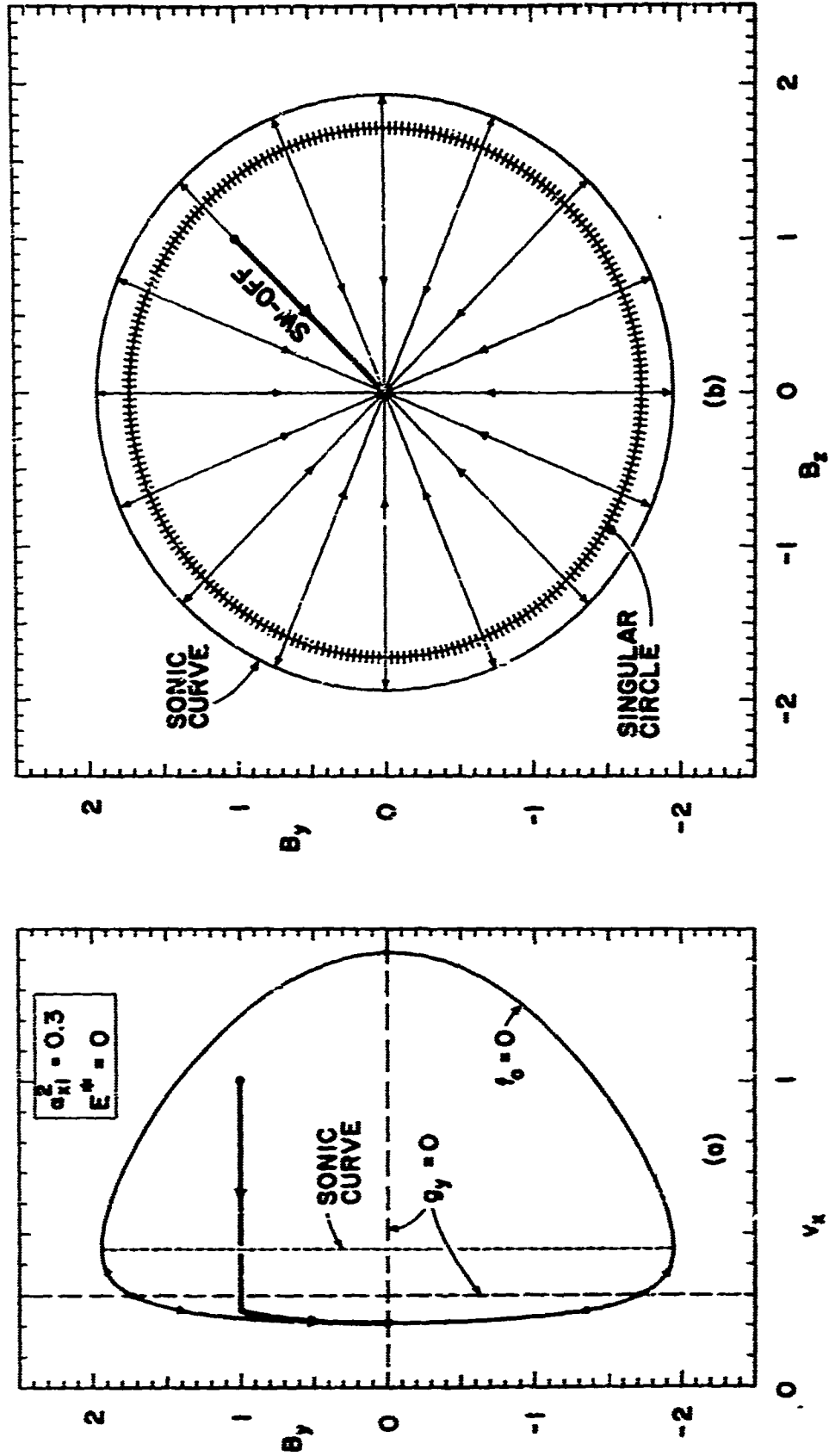
FIGURE A.4. Plane-polarized switch-off shock wave structure for $E^* = 0$. Note the unusual circular singular curve at $v_x = \alpha_{x1}^2$ ($= 0.3$, in this case).
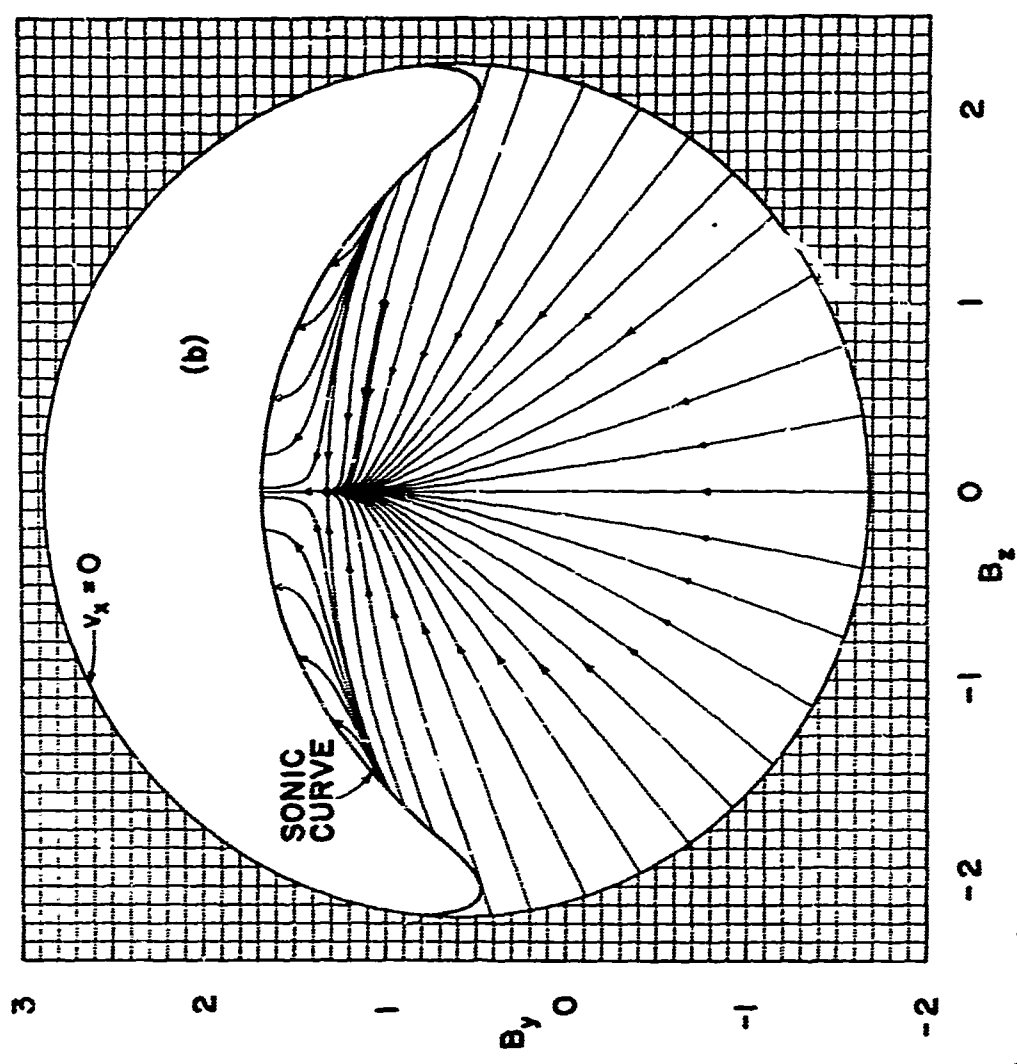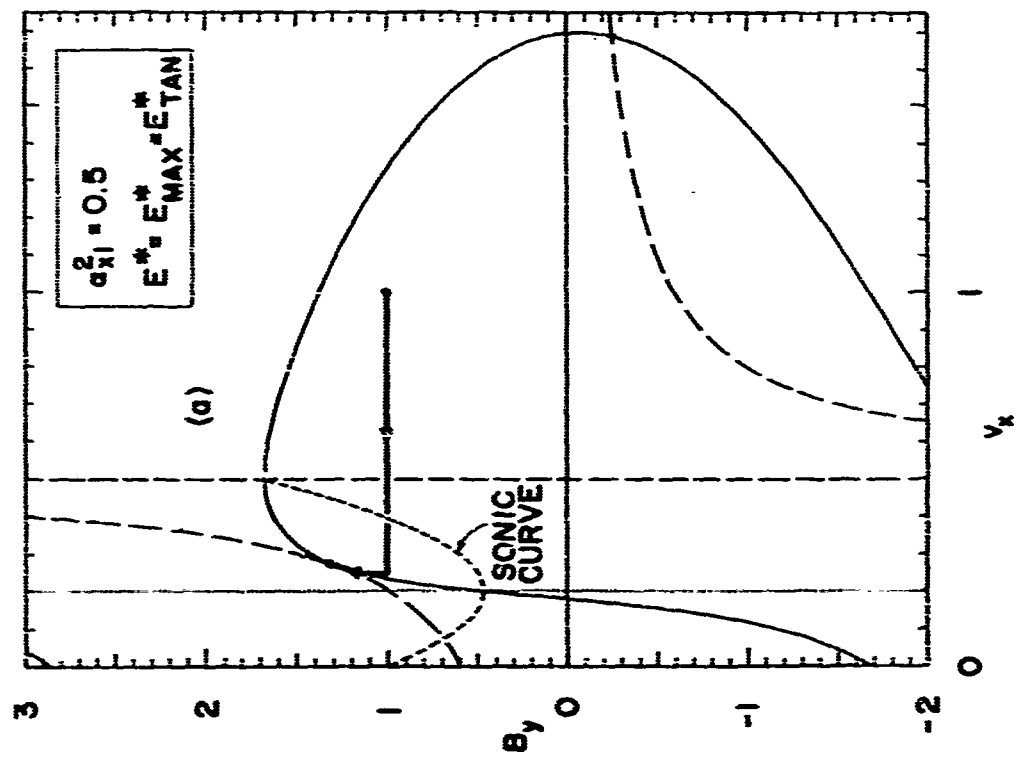
FIGURE A.5. Trajectories for $E_{MAX}^* = E_{TAN}^*$. Note the hybrid singularity which has saddle-point characteristics on one side, and nodal characteristics on the other.

in this case has saddle-point behaviour above the separatrix
and nodal behaviour below. As mentioned in §3.3, the up-
stream point must lie within the separatrix, as shown, for
a Chapman-Jouguet solution to exist. A similar situation
occurs for the usual type of E^*_{MIN}, except the position of
the singularity is well below B_{y1} (and possibly below $B_y = 0$)
and the form of the singularity is the inversion of that shown
in figure A.5. This singularity has some rather interesting
properties in that it cannot be linearized locally, and tra-
jectories entering on the nodal side do so only extremely
slowly (as if they were being "pushed away" by the outgoing
tendencies of the saddle-point side).

REFERENCES

COWLEY, M.D. 1967 J. Plasma Phys. 1, 37.

KUNKEL, W.B. & GROSS, R.A. 1962 Plasma Hydromagnetics (ed.
D. Bershader), pp. 58 - 82. Stanford University Press.

LEONARD, B.P. 1966 Phys. Fluids 9, 917.

LEONARD, B.P. 1969 Phys. Fluids 12, 1816.

LEONARD, B.P. 1970 (a) Phys. Fluids 13, 833.

LEONARD, B.P. 1970 (b) Columbia University Plasma Laboratory
Report Number 50.

SHERCLIFF, J.A. 1965 A Textbook of Magnetohydrodynamics.
Pergamon Press.

TAUSSIG, R.T. 1965 Phys. Fluids 8, 1616.

TAUSSIG, R.T. 1967 Phys. Fluids 10, 1145.

VAN DYKE, M. 1964 Perturbation Methods in Fluid Mechanics.
Academic Press.